Energy Advances

ROYAL SOCIETY OF CHEMISTRY

REVIEW ARTICLE

View Article Online
View Journal | View Issue

Cite this: *Energy Adv.*, 2022, 1, 842

Understanding the role of metal supported on TiO_2 in photoreforming of oxygenates

Imran Majeed,[ac] Hassan Ali,[c] Afifa Idrees,[b] Ayesha Arif,[b] Warda Ashraf,[d] Shahid Rasul,[e] Mohd Adnan Khan,[f] Muhammad Arif Nadeem [c] and Muhammad Amtiaz Nadeem *[g]

To achieve net-zero targets regarding GHG emissions by 2050, the identification of sustainable energy vectors is critical. In this context, photoreforming presents a potential candidate for recycling and transforming widely available biomass-derived wastes into clean hydrogen fuel, such as crude glycerol from biodiesel and a potential future H_2 production opportunity from bioethanol. Many years of work has proved that TiO_2 is an excellent material for photoreforming of organics due to its stability, availability, and environmentally friendly characteristics as compared to other semiconductors. However, photoreforming faces several obstacles, including the comparatively low hydrogen generation under Sun-equivalent light sources and the need of expensive noble metals. Efforts have been made in several directions, such as extending light absorption by TiO_2 to the visible range, reducing the recombination rate of charge carriers, and preventing back reactions. To overcome these challenges, many methods have been proposed, such as controlling the phase and morphology of TiO_2 nanoparticles, decoration with various metal co-catalysts, doping with metal and non-metal ions, plasmonic enhancement, and preparation of composite systems. Although each approach has its own merits, metal loading has proven to be the most effective among them all. This review provides a deep insight into the underlying role of metal towards the enhancement of TiO_2 catalytic activity, focusing on the findings of recent published work. We discuss in detail the effect of various metals on TiO_2 electronic structure, preparation methods, role in light absorption (surface Plasmon resonance) and chemical changes during various photoreforming steps. Following this we extend our discussion to dye sensitized systems and catalyst testing benchmarking. At the end of the review, we provide possible future research directions to enhance the photocatalytic activity of TiO_2 based photocatalysts for photoreforming.

Received 17th May 2022,
Accepted 20th September 2022

DOI: 10.1039/d2ya00110a

rsc.li/energy-advances

Introduction

There is a range of reviews available on TiO_2 photocatalysis as a whole[1] photocatalytic system or with a focus on its individual aspects such as mechanism and materials,[2] modifications,[3] applications,[4] and synthesis[5] among others. However there is lack of literature available which is solely focused on the role of metal in photoreforming of organics. In this review we have focussed our discussion on unique aspects related to the role of metal thus providing thorough understanding. Photoreforming is a process that involves harnessing the redox ability of photocatalysts upon illumination, to simultaneously drive the reduction of H^+ into hydrogen gas and oxidation of organic compounds.[6] In general the process can be represented using eqn (1).

$$C_xH_yO_z + (2x - z)H_2O \rightarrow (2x + y/2 - z)H_2 + xCO_2 \quad (1)$$

When TiO_2 is irradiated with light of suitable wavelength, the valence electrons are promoted to conduction band (CB) and because of dissimilar parity, the transition probability of e^- to the valence band (VB) decreases leading to reduction in the probability of e^-/h^+ recombination.[7,8] This state of semiconductor is called excited state. After excitation electrons and holes separate and migrate to the surface of semiconductor particle. At the surface of semiconductor electrons reduces the proton to hydrogen and holes oxidizes the water to oxygen.[9] A schematic diagram of this process is shown in Fig. 1.

[a] *Applied Chemistry Laboratories, PAEC, Islamabad, Pakistan*
[b] *Department of Chemistry, GC University, Lahore, Pakistan*
[c] *Department of Chemistry, Quid-i-Azam University, Islamabad, Pakistan*
[d] *Department of Chemistry, University of Management & Technology, Lahore, Pakistan*
[e] *Faculty of Engineering and Environment, Northumbria University, Newcastle Upon Tyne, UK*
[f] *Department of Chemical and Materials Engineering, University of Alberta, Edmonton, Alberta, Canada*
[g] *SABIC-Corporate Research and Development (CRD) at KAUST, Thuwal, Saudi Arabia. E-mail: NadeemMI@SABIC.com*

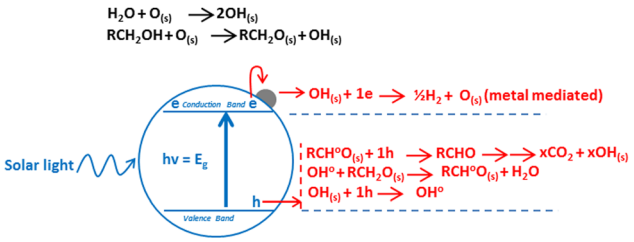

Fig. 1 Mechanism of hydrogen production by oxygenate photoreforming.

The transfer of charge to reactant can only occur when the charge carrier (electron) is higher in energy (or more negative in terms of electrochemical potential) than the electron acceptor, and the charge carrier (hole) is low in energy (more positive in terms of electrochemical potential) than the electron donor, thus allowing electron and holes flow.[10] Photoreforming can become a cheap and versatile process for hydrogen production under mild conditions from biomass. Oxygenates such as ethanol are an interesting source of hydrogen (eqn (2)), as they can be considered both as a model substrate[11] and as an industrial feedstock from waste or energy crops (cellulosic ethanol).

$$C_2H_5OH + 3H_2O \rightarrow 2CO_2 + 6H_2 \quad \Delta G^{\circ} = +137 \text{ kJ mol}^{-1} \qquad (2)$$

As for the photoreforming reaction of ethanol, two perspectives can be considered. On the one hand, the photoreforming reaction allows the direct storage of solar energy in molecular hydrogen bonds. Since solar energy is abundant and free, this process is more sustainable than the state of the art in thermocatalytic ethanol steam reforming, which uses heat as an energy source, usually by burning a fuel. On the other hand, ethanol could be a hydrogen storage medium that can be converted to hydrogen using on-board reforming technology

Imran Majeed

Dr Imran Majeed is currently working in the Pakistan Atomic Energy Commission in Islamabad, Pakistan, as a Principal Scientist. In 2018, he received his PhD from the Department of Chemistry at Quaid-i-Azam University in Islamabad, Pakistan. His PhD research focused on employing visible light active TiO_2 based photocatalysts to produce hydrogen from renewable sources. Imran has published over 20 papers related to hydrogen production using non-noble metal supported TiO_2 and CdS photocatalysts.

Hassan Ali

Hassan Ali is currently a PhD scholar in the Department of Chemistry, Tsinghua University, Peoples Republic of China. In 2015, He received his master degree (M. Phil) from the Department of Chemistry at Quaid-I-Azam University, Islamabad, Pakistan. He obtained his Bachelor degree from the Department of Chemistry, The Islamia University of Bahawalpur, Pakistan in 2009. His Master degree research focused on the developing graphene based electroactive nanomaterials for fuel cell applications. Hassan has more than 10 research papers related to hydrogen production from electrocatalysis/photocatalysis.

Shahid Rasul

Dr Shahid Rasul is currently working as lecturer at Northumbria University, New Castle, UK. His major research focus is to develop efficient energy conversion and storage devices by photo-electrochemical processes for sustainable and renewable fuels. He conducts fundamental research in science and engineering of energy materials. He has expertise in designing the surface and bulk properties of materials in such a way that improves the energy efficiency of both energy conversion and storage devices.

Mohd Adnan Khan

Dr Mohd Adnan Khan is an Assistant Professor in the Chemical and Materials Engineering Department at the University of Alberta. Adnan has nearly a decade of experience working along the value chain of hydrogen and clean technology development. His research interests span catalyst development for photo-electrocatalytic renewable fuels production, advanced materials characterization, and modelling of energy systems.

in transportation vehicles. In this case, a more concentrated light source would be required (*e.g.*, a lamp or a LED device). Given the low performance of fuel cells to date, the latter may be considered a long-term prospect. While an efficient process is of course a prerequisite for industrial scale applications, *i.e.* a high hydrogen yield at the lowest possible cost, a sustainable process is an important goal for future society in order to reduce the impact of human activities on the environment. In particular, a holistic view must be taken into account.

From thermodynamic point of view, any semiconductor–organic molecule couple that satisfies requirements shown in Fig. 1 can be used for photoreforming. However, under realistic conditions other considerations including surface area, absorption coefficient, chemical stability, photo-corrosion, overpotential, electron–hole pair recombination rate and their mobility also become important.[12] The reaction rate depends on how efficiently electrons and holes move to the surface of catalyst and subsequently transferred to the reactants at surface before they recombine.[13–15] Thus, suitable surface and bulk properties are required for effective photocatalysis.[16] Among many available photocatalysts TiO_2, due to its inherent superior properties, promises to be the ideal candidate to compromise among these requirements. It is a large band gap semiconductor, with band gaps of 3.2, 3.02, and 2.96 eV for the anatase, rutile and brookite phases, respectively.[17–21] Anatase and rutile have strong absorptions around 380 and 410 nm respectively, which can be calculated by formula $\lambda = 1239.8/E_{bg}$.[22] Regardless of all its merits, TiO_2 still struggles with its lower activity, which is mainly due to the rapid recombination of electrons and holes. One way to solve this problem is to modify TiO_2 with metals. A five-decade research effort finally led to the realisation that an order of magnitude enhancement in the activity of TiO_2 is required for any commercial application.[23] In the following discussion, we will discuss the role of metals in reducing the electron–hole recombination and thus increasing the reaction rates.

Modifications of TiO_2 photocatalyst has often been used to increase its photocatalytic activity by decreasing the recombination rate and extending the photoresponse into visible region. Loading of noble metal on TiO_2 is more advantageous compared to other sensitization techniques such as dye molecules sensitization,[24] since noble metal deposits are relatively stable even under photoirradiation in an oxidation environment.[25–31] In general, there is an optimum loading concentration (less than 4 wt%), above which the observed photocatalytic activity decreases.[32,33] Larger amount of metal leads to a drastic decrease on the photocatalytic activity which may have contribution from metal shadowing effects to reduce the light absorption by TiO_2 and possibility that metal loading above the optimum value may cause the metal deposits to behave as recombination sites due to an excessive negative charge which can attract positive holes.[34,35] In general, metals can increase the photocatalytic activity of TiO_2 due to Schottky barrier formation or Surface Plasmon mechanism.

Schottky barrier formation mechanism

The highly improved separation of photogenerated charge carriers in TiO_2 is achieved by the formation of rectifying Schottky barrier at the interface due to energy difference between the conduction band of semiconductor and work function of the metal.[36–40] The Schottky barrier only allows the one way transport of electrons from bulk TiO_2 to the noble metal *e.g.* Pt until their Fermi levels (E_Fs) are aligned and a thermodynamic equilibrium is reached (Fig. 2).[14,41–46] When the catalyst is further exposed to light source, the photogenerated electrons can cause a shift of the E_F of TiO_2 to

Muhammad Arif Nadeem

Dr Muhammad Arif Nadeem obtained his PhD from University of New South Wales, UNSW, Sydney, Australia in 2011. He started his career as Assistant Professor at the Department of Chemistry, Quaid-i-Azam University (QAU), Islamabad, Pakistan. In 2016, He was awarded Alexander von Humboldt (AvH) postdoctoral fellowship. He worked as an AvH fellow at the Institute of Inorganic Chemistry, RWTH University, Aachen, Germany. His research program focuses on the rational design of molecular and nano-materials for (1) photocatalytic water splitting and (2) fuel cell applications. Currently, He is working as an Associate Professor of Inorganic Chemistry at QAU, Islamabad.

Muhammad Amtiaz Nadeem

Dr Muhammad Amtiaz Nadeem is a Lead Scientist at Saudi Basic Industries Corporation's Technology Center, at King Abdullah University of Science and Technology, Saudi Arabia. He has over 45 articles to his credit and 14 years of experience working on H_2 production from renewables. Before joining SABIC in 2014, he worked as an Assistant Professor at Quaid-i-Azam University in Islamabad for two years. His PhD thesis has been placed in Dean, Faculty of Natural Sciences, University of Auckland theses excellence list, later also nominated for University of Auckland best thesis award for 2012. His main research interests include surface science, photo and thermal catalysis, PV-electrolysis and industrial catalysis.

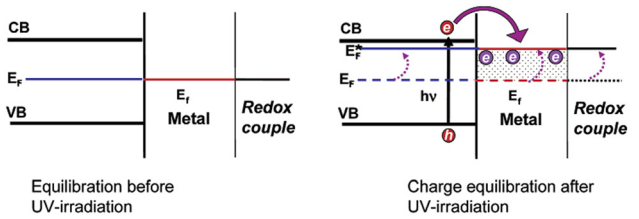

Fig. 2 Charge distribution between TiO_2–metal nanoparticles leading to equilibration with the C_{60}/C_{60}^- redox couple, before and after UV irradiation. Reprinted with permission from American Chemical Society.[52]

form a new quasi-Fermi level (E_F^*).[47] At the same time, the previously formed thermodynamic equilibrium state is destroyed, and consequently the electrons continuously migrate from the TiO_2 to the metal. By transfer of electron from semiconductor to metal the Fermi level of metal semiconductor composites shifts to more negative potential depending on the size and nature of the nanoparticles.[48–51] Small size metal particles are more effective in upward shifting of Fermi level.[52] A Fermi level shift from 20 mV for 5 nm to as large as 100 mV for 2 nm Au particles has been experimentally observed.[52–54]

Such a shift in the Fermi level enhances the efficiency of interfacial electron transfer to adsorbed species on the catalyst surface and causes a large build up in the capacitance of the Helmholtz layer and the diffuse double layer. The excess electron density remains mainly on the metal islands because the Helmholtz capacitance of the metal–solution interface is much higher than the space charge capacity of the metal semiconductor nanoparticles interface, even under accumulation contact.[55] Hence, one can expect the metal Fermi level to shift close to the bottom of the semiconductor conduction band.[52,54] Thus, H^+ ions reduction to H_2 over the noble metal surface is easier and more efficient than over bare TiO_2.[48,56,57] The work functions of the metals Pt, Pd, Au, Rh, Cu, and Ag are, 5.64, 5.12, 5.1, 4.98, 4.65, and 4.26 eV, respectively, and are larger than that of TiO_2 (4.2 eV). The enhanced performance of Au, Pd and Pt towards photocatalytic H_2 production during photoreforming may relate to their high work functions and thus Schottky barrier.[58–60] These studies also elucidate the indirect role of metals in improving the charge separation as well as promoting the interfacial charge transfer kinetics in semiconductor photocatalysis.[193,195]

The height of the Schottky barrier at the Au/TiO_2 junction decreased from 0.4 to 0.15 eV with the addition of more Au, from 0.25–2 wt%, according to the XPS examination of the valence band maxima. Because of this, compared to Au ensembles in TiO_2 + 0.25% Au composite, visible-light-generated ''hot electrons'' in TiO_2 + 2% Au composite must overcome a lower energy barrier during injection into the TiO_2 support. Because they do not accumulate at the Schottky barrier, the ''hot electrons'' in the TiO_2 + 2% Au composite are less accessible for recombination with the holes produced by visible light.[61] It is found that the conduction band electron transfer from TiO_2 to Au cocatalysts under ultraviolet light irradiation and the hot electron injection from plasmonic Au into the CB of TiO_2 with the excitation of Au by visible light are both enhanced by the formation of the Au/TiO_2(101) interface, which lowers the height of the Schottky barrier in comparison to the Au/TiO_2(001) interface.[62] Based on first-principles calculations, a thorough investigation of the effects of the interfacial structure and strain on the height of the Schottky barrier of the Pt/TiO_2(001) interface has been conducted. The results of the interface adhesion energy demonstrate that two distinct interfacial structures, namely O–Pt bonding and Ti–Pt bonding, may exist experimentally for the Pt/TiO_2(001) heterointerface. Additionally, the interfacial structures produce a range of heights for the Schottky barrier as well as variations in how the height of the Schottky barrier depends on strain. In-depth analyses reveal that the substantial dependence of the TiO_2 band edges and the interfacial potential alignments on the structure and strain is the fundamental cause of these versatile modulations of the barrier height with the structure and strain. This suggests that these results are general and may be applicable to other metal/TiO_2 heterostructures.[63]

Surface plasmon mechanism

Surface plasmon resonance (SPR) can be described as the collective excitation of valence electrons of metals oscillating against the restoring force of positive nuclei when the frequency of impinging photons matches the natural frequency of these electrons.[64] The resonant photon wavelength is different for different metals.[65,66] In case of metal–semiconductor–system it depends on many other factors discussed later.[67–69] There are few known metals which exhibit resonance in the visible region; Cu, Au, Pd, Pt, and Ag. Among these metals Au and Ag are strong plasmonic metals and are mostly studied,[70,71] while Pd and Pt have very weak surface Plasmon effects. Cu is also good SPR metal but it is not stable because of the formation of surface oxides.[72] Surface Plasmon effect is shown by metals only in their zero oxidation state.[73–75] SPR can enhance the concentration of charge carriers in the metal–semiconductor system and therefore the rates of photocatalytic reactions on the surface may occur by three mechanisms.

Plasmonic noble metals nanostructures exhibit excellent mobility of charge carriers and have almost 105 times greater cross-section area than typical dye-sensitizer molecules. Furthermore, the ability to tune the resonance wavelength by changing the size or shape of nanostructures allows for the possibility of exploitation of entire solar spectrum.[76] Both particle size and the embedding medium's refractive index have an impact on the wavelength of plasmon resonance.[4,6–10,77–80] In comparison to smaller particles, the effective restoring force that the ions exert on the electrons is reduced in large particles because the surfaces are sufficiently separated from one another and the electrons require less energy to move from their equilibrium locations. One-dimensional nanostructures, in contrast to nanocubes, feature two dipole plasmonic peaks, one of which is associated with oscillating charges along the longitudinal axis and the other with oscillating charges along the latitudinal axis.[77] These

nanostructures' increased aspect ratio leads to a red shift in the dipolar longitudinal plasmonic peak as well as an increase in peak intensity. As a result, additional plasmons will be excited and their dipolar longitudinal plasmonic peaks' intensities will increase as well. For example, this phenomenon has been demonstrated both experimentally and theoretically (using the discrete dipole approximation) for silver nanobars, respectively.[77]

SPR-mediated charge injection mechanism

SPR-mediated electron injection mechanism also called hot electron injection mechanism from metal to semiconductor (M → SC) occurs when plasmonic metal nanoparticles and semiconductor are in direct contact with each other.[25,81–87] This mechanism is analogous to dye sensitization. In oxide-supported Au nanoparticles were used to demonstrate the plasmon-induced dissociation of molecular hydrogen, a phenomenon that could only be explained by the production of hot electrons inside the metal.[88,89] The characteristics of hot electrons in plasmonic nanostructures were then calculated in a number of theoretical investigations.[90–92] The majority of experimental works on hot electron-driven photochemistry, however, use metal nanostructures in contact with semiconducting material, which further adds to the complexity of interpreting charge transfer and energetics.[93] Using hybrid metal–semiconductor nanostructures, Park and co-workers demonstrated hot electron-driven CO oxidation and time-resolved transmission spectroscopy demonstrating hot carrier relaxation on pico-second time scales.[94] Using a plasmonic Au/pGaN photocathode, DuChene and co-workers demonstrated hot hole-driven photoelectrochemical CO_2 reduction.[95]

Most semiconductors of interest for photoreforming are characterized by their conduction bands between −1.0 to 0.0 V and their valence bands between 2.0 to 3.5 V (electron energy band gap between 2.0 and 3.5 eV) on the NHE scale. For noble metal nanoparticles, the energetic electron formed in the process of the SPR excitation are in the energy window between 1.0 and 4.0 eV with respect to the metal Fermi level (0 V on the NHE scale). Owing to this alignment of the electronic states, in general the plasmonic metal/semiconductor systems may allow for the transfer of energetic electrons (hot electrons) from the metal to the semiconductor only and can execute reduction half-reactions on semiconductors, such as hydrogen evolution reaction (Fig. 3). It is worth mentioning that energetic holes retained on very small plasmonic–metal particles (particles of Au of ∼2 nm diameter), have sufficient energy to drive not only the photo-oxidation of most organic molecules, even much higher energy demanding water oxidation reaction on the surface of the metal.[96] Rezvaneh reported that electron can only be transferred to TiO_2 conduction band if the Au particle size is extremely small because the mean free path of electrons in metal particles is in the order of 1–2 nm, and hence, photo-excited electrons have a low probability to escape a larger sized particle.[97] It is obvious to note that importance of each mechanism is governed by the geometric arrangements and optical properties of semiconductor and metal in the composite systems.[71,98]

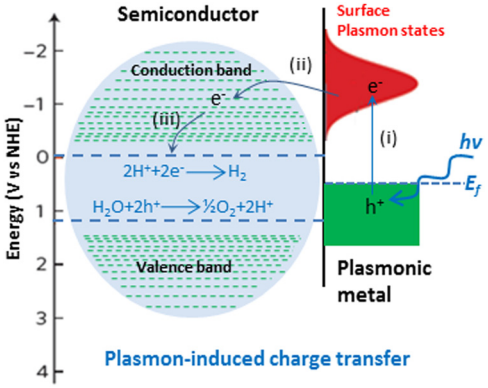

Fig. 3 Mechanism of plasmon-induced charge transfer from metal to semiconductor. I, II and III are the electronic transitions from metal to proton. Adapted from ref. 99.

Near field electromagnetic mechanism

Near field electromagnetic mechanism also called energy transfer mechanism is observed when plasmonic metal are large enough (larger than ∼50 nm in diameter) in size to generate the effective local electric field and there is a non-conducting conditions at metal/semiconductor interface preventing any direct exchange of electrons (Fig. 4).[71,100,101] Electric field induced by photo-excited metal plasmonic nanostructures are few orders of magnitude higher than the field of photons used to photo-excite the nanostructure. These fields are spatially non-homogenous, with the highest intensity at the surface of the nanostructure and decreasing exponentially with distance from the surface within ∼20–30 nm and linearly further away. As a result of this the rate of electron–hole formation near semiconductor surface increases by a few orders of magnitude. The selective formation of charge carriers in the region of the semiconductor closest to the semiconductor/liquid interface rather than in the bulk of the semiconductor offers a few critical additional advantages; (i) they are readily separated from each other under the influence of the surface potential and (ii) they have a shorter distance to migrate to reach the semiconductor/liquid interface where photocatalytic

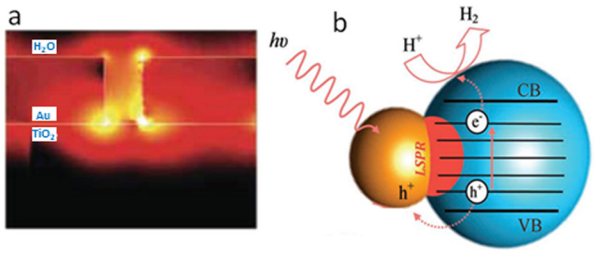

Fig. 4 (a) Optical simulations showing SPR-enhanced electric fields owing to photo-excited Au particles, permeating into a neighboring TiO_2 structure.[102] (b) Proposed photocatalytic process for efficient hydrogen generation on Au–TiO_2 nanostructures, based on near field LSPR under visible-light irradiation. Adapted from ref. 98.

transformations happens. This effectively means that the probability of photoreaction is enhanced relative to the probability of charge-carrier recombination.[99]

By combining strongly plasmonic metal nanoparticles (such as Ag, Au) with strongly catalytic metal oxide semiconductors (*e.g.*, TiO_2), redox electrochemical processes (including water splitting) have been shown to be enhanced by plasmon resonance.[71,102–104] The original interpretation of these enhancement processes was based on the local field enhancement of sub-bandgap defect-mediated absorption in the TiO_2 semiconducting material. These nanoscale metal/semiconductor systems were subjected to large-scale electromagnetic simulations using the finite difference time domain (FDTD) approach, which offered a high level of rigor. Several experimental studies, despite the great level of accuracy of these electromagnetic simulations, showed enhancement factors that were significantly larger than predicted by theory. For instance, Liu *et al.* reported a 66-fold increase in the photocurrent of an Au/TiO_2 combination at a wavelength of 633 nm, or photon energy that is roughly half the bandgap of this material, exceeding that which can only be explained by simple local field enhancement.[102]

Photon scattering mechanism

The scattering of photons by plasmonic nanostructures increases the average photon path length in plasmonic metal–semiconductor composites causing an increased rate of electron–hole pair formation (see Fig. 5).[105,106] Composite systems where plasmonic nanostructures are positioned to allow for numerous passes of resonant photons through the semiconductor matrix will exhibit very strong scattering effects.[99] The near-field electromagnetic and scattering mechanisms are important for composite photocatalysts with an overlap between metal nanoparticle SPR and semiconductor absorbance bands.[104] Ag/TiO_2 composite systems are most suitable for this mechanism because Ag shows SPR band almost in the region where doped and bare TiO_2 absorbs *i.e.* 400 to 500 nm.[71,107]

Photo-thermal effect

Photo-thermal effect has drawn some attention in heterogeneous catalysis where rate increase is observed in certain cases. On the basis of theoretical and fundamental research, postulated concepts were presented.[108] In order to investigate the impact of the plasmonic resonance response on the reaction kinetics, we previously reported the photo-thermal reactions of ethanol over Ag/TiO_2 in both steady state and ultrahigh vacuum conditions. We discovered that an increase in the reaction rate in 300–500 K temperature region was mostly due to changes in the activation energy whereas above this temperature range, the rise was caused by the pre-exponential component. The polarization of the reaction intermediates by plasmonic Ag particles, which leads to an increase in the reactivity, was suggested as a possible explanation for these findings.[109] A consistently greater hydrogen to acetaldehyde ratio during photothermal reactions in the ethanol dehydrogenation reaction, reaching the stoichiometric ratio of one, as compared to thermal reactions, suggests that H_2O generation competes with H_2 synthesis thermally. In both thermal and photo-thermal reactions, the presence of Ag speeds up the rate of H_2 evolution. This is linked to its role in H–H association reactions, in particular under light excitation which in turn might be linked to its plasmonic resonance effect (Fig. 6).[107]

Localized surface plasmon resonance (LSPR), as demonstrated by Upadhye and colleagues, can boost the reverse water gas shift reaction (RWGS) activity of Au/TiO_2 and Au/CeO_2 catalysts.[110] The improvement was attributed to changes in the catalyst surface's intrinsic reaction kinetics, either through a hot electron production mechanism or an adsorbate polarization mechanism brought on by the LSPR. Tan and colleagues found that the catalytic performance of Au/TiO_2 for ethanol oxidation increased by 50% and 100%, respectively, under visible light and UV irradiation in the photo-thermal regime (above 175 °C).[111] Under UV illumination, the rate increase was attributed to both the photo- and thermal effects equally, whereas under visible light illumination, only the plasmonic-mediated electron charge transfer from the Au deposits to the TiO_2 substrate was thought to be responsible. The photo-thermal catalytic oxidation of ethanol over TiO_2 and a 1 wt%

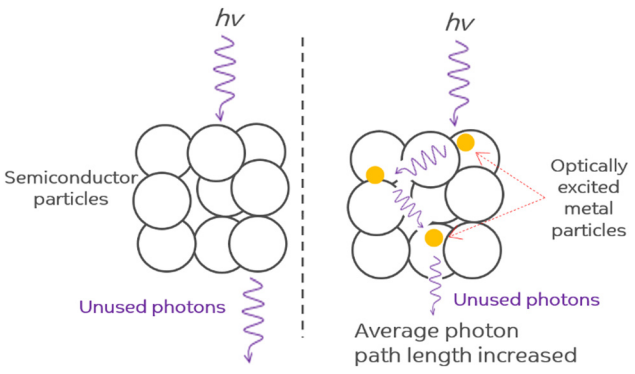

Fig. 5 Photon scattering mechanism. Adapted from ref. 99.

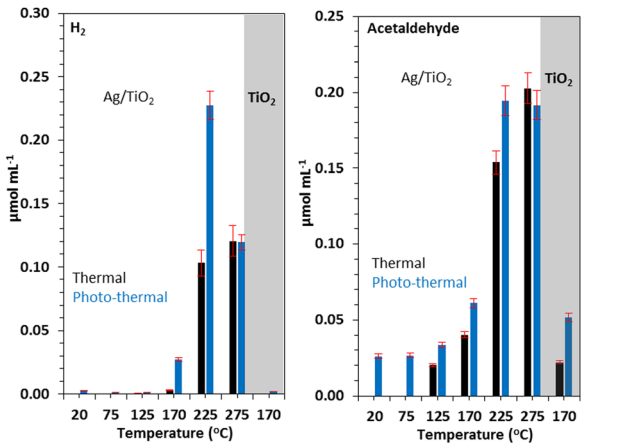

Fig. 6 H_2 (A) and acetaldehyde (B) production on similar amounts (31 mg) of TiO_2 and 3 wt% Ag/TiO_2 catalyst under thermal and photo-thermal conditions as a function of temperature at ethanol:N_2 flow rate of 5.4 mL min^{-1}. Reprinted with permission from Elsevier.[107]

Pt/TiO_2 catalyst was studied by Kennedy and colleagues. Increased levels of acetaldehyde created by photo-oxidation over TiO_2 and its subsequent interaction with Pt metal, which results in CO_2 synthesis by thermal reaction, appeared to be the main reason of the photo-thermal enhancement of CO_2 production (70 percent at 100 °C).[112]

The interaction of methanol, triethanolamine, formic acid, and glucose on Pt/TiO_2 was investigated by Song and colleagues. They claimed that the redistribution of Pt metal d-electrons to higher energy states was what caused the photo-enhancement in H_2 generation.[113] Chanmanee and co-workers investigated the alkane reverse combustion under photo-thermal conditions.[114] They noticed that the generation of liquid hydrocarbons increased as the temperature rose. On the basis of each electron stored, an incident photon quantum yield (IPQY) of 0.02–0.05 percent was attained. Hu and colleagues used black TiO_2 to study how temperature affected the visible light photocatalytic hydrogen generation from water and methanol.[115] Due to the presence of Ti^{3+} states in TiO_2 and an increase in the relative population of adsorbed methanol molecules in vibrationally excited states, the enhancement was attributed to the occurrence of visible light photocatalysis. Huang and colleagues have also proposed an improvement in the electron transfer probability and concurrent vibrational relaxation.[116]

Alternative models for the role of metal

The exact role of the metal is still disputed. In a recent paper, Zaera and coworkers presented a revolution in the role of metal in photocatalysis by introducing an alternative to the traditional approach, using the Au/TiO_2 metal semiconductor as a reference system.[117] They presented a new model in which protons from water are not reduced at the surface of the metal, a site physically separated from that on the semiconductor where oxygen production occurs. Instead, their data support a model in which the excited electrons promote the reduction of protons on the surface of the semiconductor, not the metal, and in which the reduced atomic hydrogen then moves to the metal and recombines to produce molecular hydrogen (Fig. 7).

In this study, it was found that without the ability to facilitate the recombination of hydrogen atoms, the electron trapping functionality alone cannot enhance the photocatalytic activity of the TiO_2 samples. Based on the widely accepted model for the role of the metal in photocatalysis, the focus was on finding cheaper electron scavengers. However, results show that a good catalyst for the recombination of atomic hydrogen is needed instead. For example, carbon black has been shown to be unsuitable for photocatalytic promotion despite its excellent conducting properties (the reason why it is often used as an electrode). On the other hand, nickel oxide, a material that cannot accept excited electrons from the conduction band of most photocatalysts, is nevertheless capable of enhancing their photoactivity. In general, the author believes that with a change of focus driven by this new proposed model, it may be possible to identify better promoters for photocatalysis in the near future.

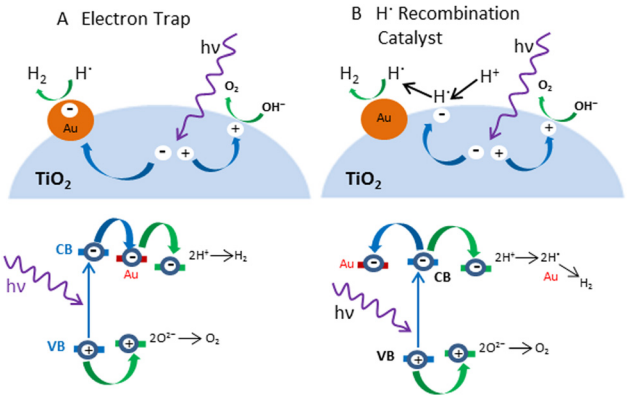

Fig. 7 Schematic representation of the mechanisms (Upper) and electronic transitions (Lower) proposed to explain the role of metals (Au) in the photocatalytic splitting of water with semiconductors (TiO_2). (A) In the conventional model, the metal acts as an electron trap that physically separates the excited electron used for proton reduction from the oxidation step that occurs on the surface of the semiconductor. (B) Alternative model proposes that H^+ reduction occurs at semiconductor sites but that the resulting hydrogen atoms need to migrate to the metal to recombine and produce the final H_2 product. Adapted from ref. 117.

Bowker and co-workers proposed a very different mechanism for the role of metal in the photocatalytic reforming of methanol on Pd/TiO_2 catalysts.[118–120] The key part of this was that the dehydrogenation of methanol on the Pd occurred even in the absence of light, but the reaction stopped because the metal surface was blocked with CO, which is strongly adsorbed on Pd. The role of light was to create an active oxygen state (probably O^-) by absorbing light through band gap excitation in the TiO_2. This oxygen was then in turn able to react with the poisoning CO to form CO_2 and sustain the conversion of methanol. The oxygen vacancy in the TiO_2 lattice was filled by the reduction of water to produce hydrogen (Fig. 8). It is likely that the mechanism

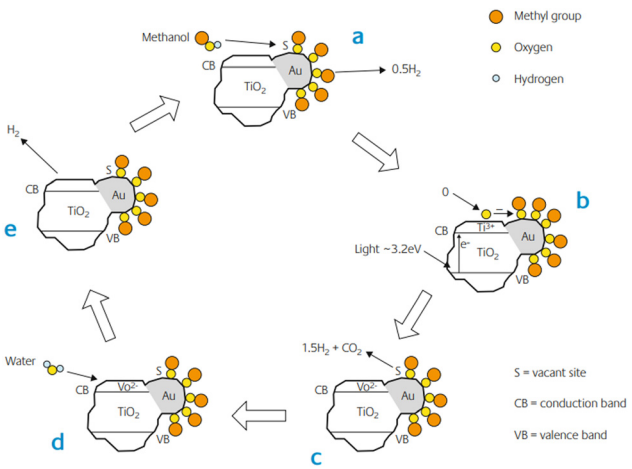

Fig. 8 The proposed mechanism of anaerobic photocatalytic reforming of methanol on Au/TiO_2. Here we show the methoxy as the pivotal intermediate in the reaction, though it could be the formate. Adapted from ref. 121.

in the case of Au/TiO_2 is different from that of Pd/TiO_2. CO is much weaker bound to the Au surface due to the low energy of the d orbitals in Au. Therefore, the blocking surface intermediate of methanol is probably different from that of Pd. The species in question could be methoxy or formate.

They showed from TPD, that format is the intermediate in Au/TiO_2, at least in an oxidising environment, leading to the simultaneous desorption of CO_2/hydrogen from the surface at ~200 °C, a property not present in TiO_2 alone. Boccuzzi and co-workers have identified both intermediates on Au/TiO_2 catalysts by infrared measurements.[122] Whether the methoxy or the formate is the key intermediate, it has been suggested that this intermediate is destabilised in the presence of light, possibly by reaction with excited species on the support. It was also found that methoxy intermediates also existed on the TiO_2 support.[122] However, these were more stable than those on the gold, produced other products (methane, CO and water) and do not appear to be affected by the presence of gold nanoparticles. Thus, they are probably spectators in the course of photocatalysis, since TiO_2 alone does not produce such products.

Pt/TiO_2: a typical benchmark

Platinum (Pt) is the most frequently used metal to modify the TiO_2 photocatalyst surface because of its suitable work function,[123] the smallest over-potential for H_2 evolution,[15,124–127] higher intrinsic platinum activity in reductive processes,[128] high activity due to smaller size (but not too small), presence of optimum electron trapping Ti^{3+} sites in Pt than Au loaded TiO_2,[129] and facilitation in the discharge of electrons from semiconductor nanoparticles into the electrolyte by forming an ohmic contact which accelerates H_2 production from water in the presence of a sacrificial electron donor.[125,130] Usually, the optimum amount of Pt loading on TiO_2 P25, a well-known reference photocatalyst, is 0.5 wt%.[131–133] It is Pt(111) face that come in contact with anatase TiO_2 (101) face to form the Pt–TiO_2 interface. The perpendicular alignment between the (111) lattice planes of Pt and (101) lattice planes TiO_2 enhance charge transfer due to better matches than the parallel alignment which makes a distorted Pt–TiO_2 interface (Fig. 9). An optimum Pt particle size is required for optimum activity. For Pt nanoparticles of about 1 nm size no injection of electrons takes place due to higher metal Fermi level whereas when the particles are too large, the Fermi level of metal is low enough that in addition to electrons, holes can also be injected from the VB of TiO_2 into the nearby energy state of the metal, hence facilitating charge carrier recombination.[134,135]

It has been reported that the photocatalytic H_2 evolution activity of Pt/TiO_2 samples is closely related with the valence state of Pt cocatalyst.[137] Metallic Pt nanoparticles may have little contribution to H_2 evolution because of too high adsorption energy.[138,139] One of the major drawbacks of photoreforming on Pt/TiO_2 is the favorable thermodynamics for water oxidation back reaction at room temperature under atmospheric pressure.[140,141] Addition of different electrolytes

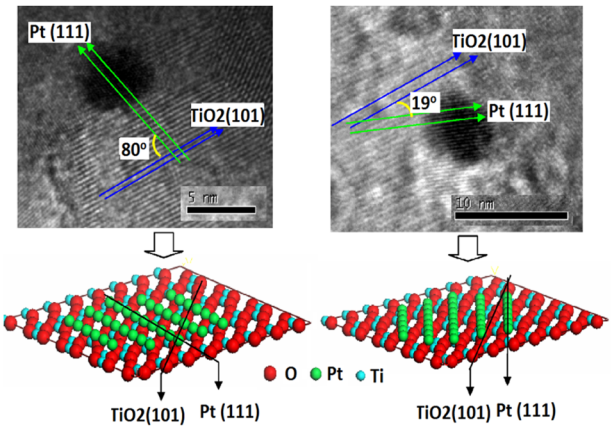

Fig. 9 High-resolution TEM images of (a) perpendicular (b) parallel; with speculated metal–support interface. Reprinted with permission from Elsevier.[136]

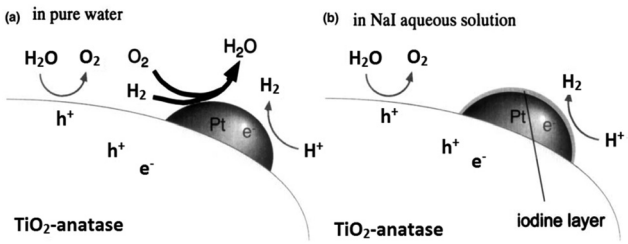

Fig. 10 Speculated reaction mechanisms over Pt–TiO_2; (a) in pure water (b) NaI aqueous solution. Reprinted with permission from Royal Society of Chemistry.[145]

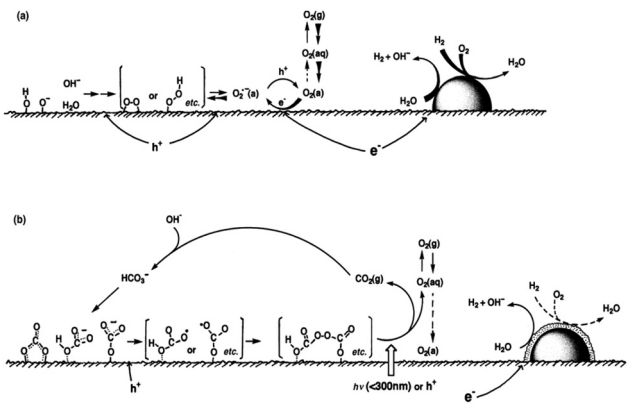

Fig. 11 Speculated reaction mechanism over Pt/TiO_2; (a) in water and (b) in carbonate salt aqueous solution. Reprinted with permission from Royal Society of Chemistry.[143]

including NaOH, Na_2CO_3 and NaI in the reaction mixture is one of the effective methods to inhibit the back reaction on Pt surface as explained in (Fig. 10 and 11).[142–145]

$Gold/TiO_2$: a recent benchmark

Electrochemical,[146] photochemical[48,147] and spectro-electrochemical[148,149] experiments have shown that the gold nanoparticles

readily accept electrons from a suitable donor or an electrode. These electrons can be further used to reduce H^+ to $1/2H_2$ when photoexcited TiO_2 is used as an electron donor. According to some reports, complete photocatalytic decomposition of water is possible using Au as compared to Pt where back reaction of H_2 and O_2 can be avoided on the former.[150] Au/TiO_2 nanocomposites exhibit two operating mechanisms including UV or visible light for water splitting depending upon the wavelength of excitation.

UV light mechanism

In the UV irradiation the efficiency of charge separation is improved by the transfer of electrons from TiO_2 to Au nanoparticles due to the formation of Schottky barrier.[45,151] Sreethawong and co-workers compared the reactivity of Au, Pd and Cu loaded anatase TiO_2 for hydrogen production and found the reactivity order as Au > Pd > Cu.[35] However loading of gold nanoparticle decreases the photocatalytic activity for the decomposition of the organic compounds due to the reduction of the surface OH groups.[152] Morphology of the gold particles in Au/TiO_2 photocatalysts has a direct effect on the photocatalytic activity. It has been reported that spherical or hemispherical gold particles are more active than rod shaped particles.[150,153–155]

Visible light mechanism

Gold surface plasmon excitation (SPR) is another mechanism responsible for the visible light driven water splitting reaction on the Au/TiO_2 photocatalyst.[81] This effect is characteristic of relatively smaller Au nanoparticles in metallic Au(0) state.[73,74] Gold nanoparticles (5–50 nm) absorb in the visible range from 500 to 600 nm due excitation of surface plasmons and may inject hot electrons into the conduction band of TiO_2.[71,156] Electrons in the TiO_2 conduction band and holes in gold nanoparticles may have appropriate potential to produce hydrogen and oxygen from water due to reduction and oxidation reaction respectively. Larger gold nanoparticles possess stronger plasmonic resonance which leads to more-intense plasmonic near-fields and hence higher optical absorption in the TiO_2 for efficient photocatalysis. Gold nanoparticles (50–70 nm) in the Janus nanostructures has been reported photocatalytically more active due to their stronger plasmonic near field effect.[98] The position, intensity and shape of the plasmonic band seen in the absorption spectra depend on various factors including particle size and morphology, loading amount, calcination temperature, dispersion, interparticle distance, and the dielectric property of the surrounding medium.[68] Gold nanoparticle <2, 2–50 and >50 nm show very nominal absorption band (almost flat), a strong absorption band in the region 520–530 nm and a wide absorption band to include the whole visible range respectively.[157] Obviously the mechanism of photochemical process indicated in Fig. 12 is an oversimplification since it has been demonstrated that there is a charge re-distribution between the gold nanoparticles and the semiconductor which causes a shift of semiconductor Fermi level toward more negative potentials.[54,82]

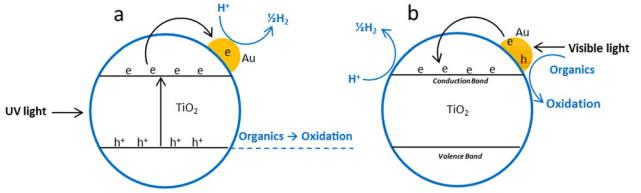

Fig. 12 Proposed photoreforming mechanism over Au/TiO_2; (a) under UV light irradiation (b) under visible light irradiation.

Au/TiO_2 photonic crystals

Photonic crystals (PCs) are a periodically structured electromagnetic medium through which light cannot propagate linearly.[158] PCs can localize, trap, provide multiple paths and magnifies light intensity at the plasmonic wavelength of the metal particles and thus enhance the SPR of the metal nanocrystals, ultimately leading to enhanced visible light hydrogen production from photo-reforming at TiO_2. The development of appropriate techniques to create artificial photonic crystal structures has received substantial attention because of their outstanding optical properties. Here, colloidal self-assembly technology,[159,160] precision machining, nanolithography,[161–163] and layer-by-layer method are the basic photonic crystal fabrication techniques.[164]

Gravity, capillary forces, or the electric and magnetic droved deposition process are the main means of achieving the self-assembly method of colloidal crystals, also known as the bottom up method. Through this technique, photonic crystals with a vast area of compact arrangement and uniform particle size can be constructed.[165,166] Regarding the precision machining method, sets of holes are drilled into solid slab or wafer surfaces using chemical beam-assisted ion etching to produce PCs.[167] The photonic crystal with the photonic forbidden band has a lattice constant up to millimeters in the microwave band, as shown by the machining technique. When constructing PCs using the layer-by-layer method, a 1D rod layer with a stacking sequence that repeats every four layers is typical. The rods are parallel and maintain a set pitch to one another in a repeating unit. Additionally, between neighboring layers, the rods' orientation is 90 degrees rotated.[168]

Zhang and co-workers synthesized unique Au loaded highly porous photonic crystals (PCs) layer of TiO_2 by facile anodization procedure in which plasmonic wavelength of Au matches the photonic band gap of the TiO_2 PCs (Fig. 13).[169] Under visible light illumination (>420 nm), the designed material produced a photocurrent density of $\sim$150 μA cm^{-2}, which is the highest value ever reported in any plasmonic Au/TiO_2 system under visible light irradiation. This work contributes to the rational design of the visible light responsive plasmonic photocatalytic composite material based on wide band gap metal oxides.

Recently, Idriss and coworkers fabricated three dimensionally ordered macroporous, inverse opal TiO_2 based Au/TiO_2 and $Au–Pd/TiO_2$ photocatalyst having photonic band gapes (PBG) centered at 357 nm coinciding with electronic band gape of TiO_2 and 580 nm coinciding with surface plasmon resonance of gold.[170] They noted that the Au/TiO_2 with the PBG position

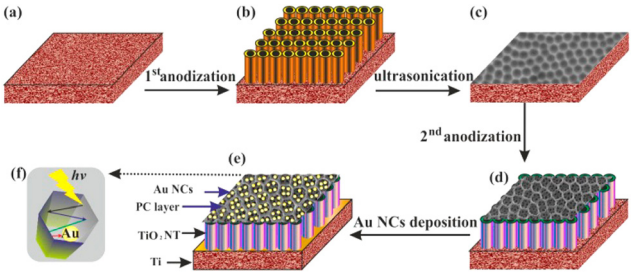

Fig. 13 Schematic diagram of the Au/TiO_2 nanotubes photonic crystal (NTPC) fabrication procedure: (a) Ti foil, (b) anodization, (c) nano imprints on the Ti foil after ultrasonication (d) second anodization, (e) Au nanocrystals deposited on the TiO_2 (NTPC) *via* photocatalytic reduction; (f) top of view of (NTPC) layer for light trapping and enhancing SPR of the Au nanocrystals. Reprinted with permission from American Chemical Society.[169]

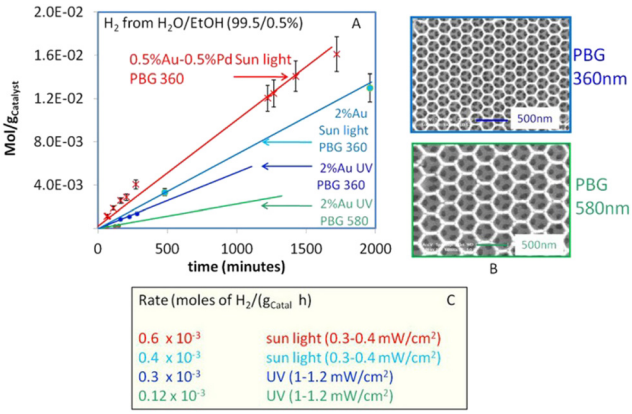

Fig. 14 (A) Hydrogen production from photoreforming of ethanol using photocatalysts with two different PBG positions under UV light with flux about 1–1.2 mW cm^{-2} and under direct sun light with UV flux of about 0.3–0.4 mW cm^{-2} (B) SEM images of the two PBG Au/TiO_2 photocatalysts (C) Hydrogen production rates (C). Reprinted with permission from Springer Nature.[170]

close to its electronic band gap is 2 to 3 times more active. The highest performance was found for the Au–Pd/TiO_2 with PBG of 360 nm. High rate of hydrogen production was attributed to suppressed e–h recombination due to the co-incidence of the photonic band gape (357 nm) with the electronic band gape (385 nm) of TiO_2 (Fig. 14).

Pd/TiO_2: a future benchmark

Palladium (Pd) is the cheapest and most commonly used metal among the noble metals (Pt, Pd & Au) as co-catalyst with the TiO_2 photocatalyst,[60,171,172] and the cost of Pd metal is approximately 20–25% of that of platinum (Pt) metal.[173] Theoretically, larger the difference between the metal's work function and that of TiO_2, larger the height of the Schottky barrier formed at the TiO_2 surface. Hence, platinum (Pt) should be more effective than palladium (Pd) or gold (Au) in accepting conduction band electrons of TiO_2, and therefore should exhibit high H_2 production activity. Recently, palladium (Pd) is emerging as an efficient metal cocatalyst compared to Au and Pt for proton reduction site because the density of states in the vicinity of the Fermi level is higher for Pd than for Pt and Au with the Fermi level of Pd being ~0.2 eV higher than the Fermi level of Pt (−10.8 eV).[174,175] Pd also has an optimum Schottky barrier height and a much lower electron affinity and hence electron trapping capability which may enable more facile electron transfer from Pd for proton reduction.[174] Additionally, high surface area offered by the Pd due to the porous nature of metallic Pd may also contribute to its high activity.[176] Su and co-workers probed the kinetics of the photogenerated electrons on metal–semiconductor photocatalyst systems and found that a fast proton reduction occurs on Pd/TiO_2 as compared to Au/TiO_2.[177] It was revealed that Pd shows a slow reverse transfer process of electrons from metal to TiO_2 (low k_{rev}) for the trapped photogenerated electrons. Since Pd most likely provides an ohmic contact, whereas Au shows capacitive properties. It is likely that a combination of the above factors is important to the superior performance of the Pd/TiO_2 relative to Pt/TiO_2 or Au/TiO_2 for hydrogen production through photoreforming of oxygenates. There are some others reports in literature where Pd is used as cocatalyst over TiO_2 for hydrogen productions reactions.[58,60,171,173]

Alkaline earth metal oxide (AEMO), usually regarded as structural promoters, can also promote the photo-catalytic activity of TiO_2 by raising its Fermi level.[178,179] It was also reported that the AEMO incorporated into M/TiO_2 stabilizes the size of metal nanoparticle by making an alkaline earth metal, noble metal and Ti metal mixed oxide layer at metal–TiO_2 interface. This layer acts as glue at metal–TiO_2 interface thus preventing sintering.[180,181] Our group recently explored the role of alkaline earth metal oxides in palladium supported TiO_2 photocatalysts. It was observed that very high rates of hydrogen production can be achieved by the introduction of AEMO in metal supported TiO_2 photocatalysts.[51,182] Alkaline Earth Metal Oxides (AEMOs) promoted electron transfer from the TiO_2 surface to palladium nanoparticles by raising Fermi level of TiO_2 (from E_F to E_F^*) and the conduction band level (from E_{CB} to E_{CB}^*) due to more negative potential for SrO/TiO_2 support as compare to TiO_2 alone (Fig. 15). It was found in XPS studies

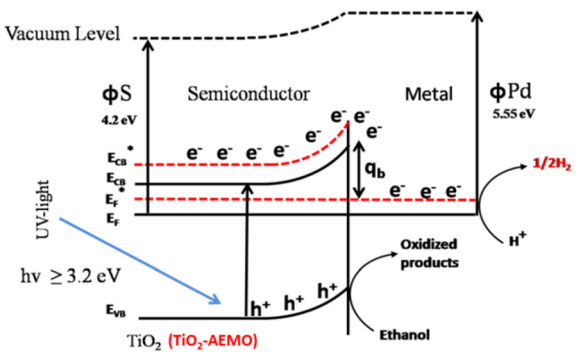

Fig. 15 Schematic illustration of electron transfer between Pd and AEMO-TiO_2. Reprinted with permission from American Chemical Society.[182]

that palladium nanoparticles were exclusively in metallic state due to close proximity of highly electropositive AEMOs (SrO, BaO) which is highly beneficial for palladium to act as proton reduction sites. Yang and Co-workers also described such promotion of electrons transfer from SrO/TiO_2 surface to active metal sites by the elevation of Fermi level for rapid CO oxidation reaction.[183]

Non noble metal supported TiO_2

Precious metals are expensive and rare, which makes their future doubtful. Therefore, it makes sense to develop substitutes that are free of precious metals. Ni and Cu as substitute have been studies in this regard.[184–186] Although all reported hydrogen generation rates over these photocatalysts are still low from an economic and practical point, however, they are strong candidates to replace highly expensive Pt and Au co-catalysts for solar H_2 production. Some of the important work related to role of these metals in photoreforming is discussed.

Cu_2O/TiO_2

Cu_2O is one of the few p-type direct band gap (2.0–2.2 eV) semiconductors which are inexpensive, nontoxic and readily available.[35,187–195] The coupling of Cu_2O with TiO_2 not only enhances the photocatalytic activity of TiO_2 but also extends the optical response from UV to visible range. Cu_2O/TiO_2 composites systems having appropriate energy levels with respect to both oxidation and reduction of water are reported to produce hydrogen under visible light irradiation.[139,196–200] Cu_2O as a p-type semiconductor when combines with a n type semiconductor (TiO_2) makes a hetero-junction of type II-staggered in Cu_2O/TiO_2 composites. When visible light is supplied to this nanocomposite, electrons in the conduction band of p-type semiconductor will be thermodynamically transferred to the conduction band of n-type semiconductor and holes remain in the valence band of p-type semiconductor. In the presence of metal such as Au and under UV irradiation, both electron and hole can transfer from TiO_2 to Cu_2O (Fig. 16).[201,202]

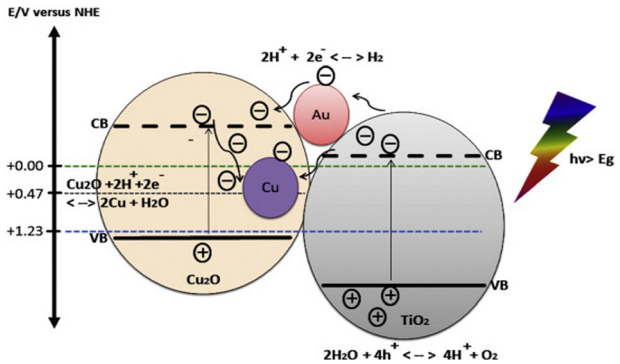

Fig. 16 Energy band position of Cu_2O and TiO_2 aligned with redox potential of water. Reprinted with permission from Elsevier.[210]

The migration of photogenerated charge carriers can also be promoted by the inner electric field established at the hetero-junction interfaces also known as space charge regions.[203–206] Consequently, the recombination rates of photogenerated charge carriers will be greatly suppressed which is resulting into high photocatalytic activity.[201,207] Sinatra and co-workers observed 10 times greater rate of hydrogen production over 2% Au–Cu_2O/TiO_2 than 2% Au–TiO_2 from glycerol water mixtures due to the synergetic effect of the Cu_2O/TiO_2 p–n junction and noble metal nanoparticles.[208] Cu_2O/CdS nanostructures were also reported to have superior photocatalytic hydrogen production from water splitting due to type II hetero-junction formed at the Cu_2O/CdS interfaces.[209]

Zhang and co-workers studied that the deposition potential during electrodeposition of Cu_2O on TiO_2 nanotubes array (TNA) has direct effect on the morphology and visible light hydrogen production activity of as prepared Cu_2O/TiO_2 nanotubes array photocatalysts.[211] Cu_2O electrodeposited at −0.8 V had maximum exposed (111) facets and was found to have better photocatalytic activity (42 times) for hydrogen production from water–glycerol mixture. Among (110), (111), (200) and (220) planes of cubic Cu_2O, (111) facet is the most stable and is proposed to hinder oxidation of Cu^{1+} to Cu^{2+}. Xi and co-workers demonstrated that Cu_2O/TiO_2 photocatalyst prepared by glucose solvothermal method generated 16 times greater hydrogen form ethanol–water mixture than P25 under visible light due to the reduction of a part of Cu_2O to Cu^0 and the synergistic effect of Cu_2O and Cu (Fig. 17). The photogenerated electrons first transferred to Cu and then to the conduction band of TiO_2, which enhanced the lifetime of photogenerated charge carriers. As a result of this synergistic effect hydrogen evolution rate on $Cu_2O/Cu/TiO_2$ was twice as on Cu_2O/TiO_2.[212]

Lalitha and co-workers reported the highest rate of hydrogen production to date from 5% glycerol water system under solar light irradiation over Cu_2O/P25 photocatalyst. However, the mechanism of charge dynamic was not clear in their study.[213] Very recently our group deposited highly dispersed Cu–Cu_2O nanoparticles over TiO_2 by using metal organic frameworks as templating agents to prevent agglomeration of Cu ions as it happens when metal salt is used. It was observed that Cu_2O was reduced to metallic Cu due to the rise of TiO_2 conduction band electrons E_f level under continues UV excitation, and under visible light Cu_2O established the p–n junction where only electron transfer occurred from Cu_2O to TiO_2. In both cases hydrogen production rate was very encouraging.[214]

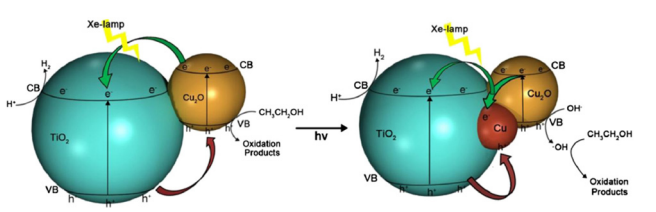

Fig. 17 H_2-Production mechanism form photoreforming of ethanol using $Cu_2O/Cu/TiO_2$ under Xe-lamp irradiation. Reprinted with permission from Elsevier.[212,214]

CuO/TiO_2

CuO deposited over TiO_2 has been found to markedly enhance hydrogen production activity as compared to pure TiO_2,[199,215–217] even sometimes more than noble metal based photocatalysts.[218] A considerable negative shift in Fermi level of the CuO by the transfer of electrons from TiO_2 is responsible to gain the necessary potential for hydrogen production on CuO. Decrease in hydrogen production rates over Cu/TiO_2 photocatalyst with time is attributed to the adsorption of sacrificial reagents oxidation products over photocatalyst active surface and due to decrease of Cu contents due to drop of pH by the formation of CO_2. A decrease in Cu content from 9.1 to 8.1 mol% has been observed due to Cu leaching at 5.6–4.6 drop in pH. Gombac and co-workers prepared unique design of catalyst by covering the CuO_x with porous TiO_2 using water-in-oil micro-emulsion method for hydrogen production from organic species. The superior activity of this system was due to the combined effect of fine Cu/CuO_x dispersion and possibility of some Cu incorporation into the TiO_2 lattice. Stability tests under reducing conditions in the presence of a sacrificial agent indicate that copper leaching was marginal. Major issue confronted while using Cu and Ni as cocatalyst is the formation of agglomerates which enormously reduce the hydrogen production rates. In this context, a remarkable breakthrough was brought by Young and Co-workers who deposited the highly dispersed Cu nanoparticles for the first time by complex precipitation method.[219] In this innovation Cu–glycerol complex was developed which was later precipitated by strong alkali. It has been also validated later that bulk CuO has positive conduction band potential than H^+/H_2 redox couple. However, smaller CuO nanoparticles have different electronic band structure and conduction band potential becomes negative compared to H^+/H_2 redox couple due to quantum confinement effect.[220–222]

Idriss and co-workers explored above results further by depositing the Cu nanoparticles over TiO_2 by following the method as described by the Young and Co-workers. They found that the activity of CuO/TiO_2 was found to depend on the nominal CuO loading, with 1.25 wt% CuO being optimal (H_2 production rate = 20.3 mmol g^{-1} h^{-1} in 80 : 20 EtOH : H_2O).[223] At this loading amount, a highly dispersed sub monolayer Cu(II) species on TiO_2 surfaces rather than supported CuO nanoparticles were proposed as the active site for hydrogen production. The Fermi level for such adsorbed species is positive with respect to the TiO_2 conduction band but negative than H^+/H_2 redox couple. For CuO nanoparticles of size ~3–4 nm, the band gap is around 2.3–2.6 eV as compared to bulk CuO, E_g ~ 1.3–1.5 eV. As the CuO nanoparticle size increases, the conduction band of CuO becomes positive with respect to H^+/H_2 redox couple, preventing direct transfer of electrons from CuO to H^+ and H_2 formation is suppressed accordingly. The inactivity of bulk CuO for H_2 production can be explained using the same rationale (Fig. 18). These results have also been confirmed by latest research by Jung and co-workers. At an optimum Cu loading of 0.5 wt% the CuO_x was present as relatively highly dispersed fine nanoclusters. At Cu loadings beyond 0.5 wt% a

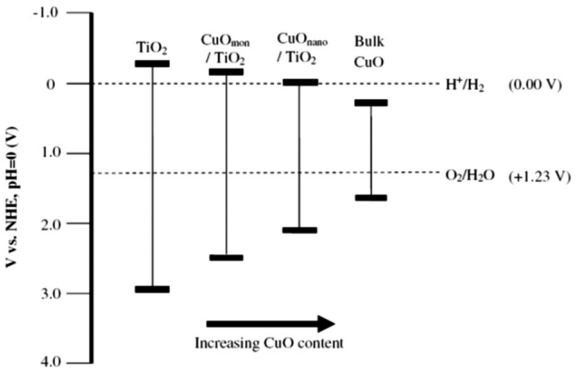

Fig. 18 Band gap energies for TiO_2, CuO and CuO/TiO_2 photocatalysts with respect to CuO loading. Reprinted with permission from Elsevier.[223]

bimodal distribution of CuO_x deposits appeared with the prevalence of larger Cu deposits increasing with increasing Cu content.[224] Our group recently described another method to deposit highly dispersed Cu nanoparticles by using metal organic frameworks (MOFs).[225] A Cu based MOF was first deposited over TiO_2 then as prepared composite was calcined at various temperatures to get highly dispersed Cu nanoparticles. In this study intermediate carbon was proved helpful in reduction of Cu^{2+}/Cu^0 during calcination process.

The $Cu(OH)_2/TiO_2$ systems have recently shown some good results for hydrogen production. Yu and co-workers fabricated $Cu(OH)_2/TiO_2$ photocatalysts using the deposition precipitation using NaOH and reported a hydrogen production rate of 3.4 mmol h^{-1} g^{-1} in a 0.09 M ethylene glycol solution under UV irradiations.[226] The potential of $Cu(OH)_2/Cu$, ($Cu(OH)_2$ + 2e = Cu + 2-OH, E° = −0.224 V) is slightly lower than conduction band (−0.26 V) of anatase TiO_2 and higher than the reduction potential of H^+ ($2H^+ + 2e = H_2$, E° = 0.000 V), which favors the electron transfer from the CB of TiO_2 to $Cu(OH)_2$ which causes the reduction of Cu^{2+} to Cu^0 nanoclusters (Fig. 19). These Cu^0 clusters promote the transfer of photo-generated electrons from the conduction band of TiO_2 to reduce H^+.[184,185]

In general, the systems where metal in loaded during TiO_2 synthesis step from its precursors outperform the impregnated systems that used either ethanol or glycerol as sacrifice molecules, demonstrating better hydrogen production rates.[227]

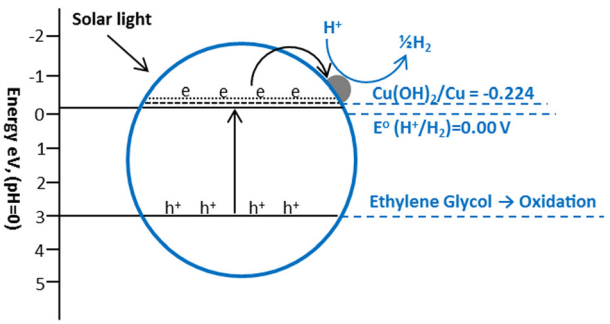

Fig. 19 Proposed mechanism of hydrogen production from ethylene glycol over $Cu(OH)_2$ loaded TiO_2.

By photodepositing Cu on the surface of TiO_2 supports, active and affordable nanocomposites can be created. TiO_2 structural characteristics have a significant impact on its activity, for example, highly defective surface results in a very high dispersion of the metal and a higher activity for H_2 production due to an increase in the oxidation rate of the sacrificial agents. While solar-like radiation causes a significant portion of the Cu to be oxidized and prone to photocorrosion, UV light only causes little leaching.[228] After a few hours, the concentration of Cu ions stabilizes, indicating that an equilibrium has been reached between the leaching phenomenon and the Cu photodeposition process. Surprisingly, there is little of a detrimental impact on hydrogen generation.[228] Cu^{2+} ions partially enter the TiO_2 structure in CuO_x/TiO_2 nanocomposites made *via* copper photodeposition, which causes oxygen vacancies to form and alter the band gap while also creating traps for photogenerated holes and electrons. Compared to liquid-phase procedures, gas-phase processes provide higher H_2 productivity and, in particular, higher selectivity (approximately 92–93%) to acetaldehyde.[229]

Ni/TiO_2

Recent studies have shown that nickel is a good choice for the preparation of active TiO_2-based catalysts for hydrogen production compared to other transition metals. However, the mechanism behind the enhancement of photocatalytic activity is more complex. Different mechanisms have been proposed depending on the type of nickel such as Ni, NiO or $Ni(OH)_2$. Yu and co-workers deposited $Ni(OH)_2$ nanoclusters on TiO_2 by a simple precipitation method and observed a hydrogen production rate of 3.0 mmol h^{-1} g^{-1} in 25 vol% aqueous methanol under UV excitation.[230] The hydrogen evolution was attributed to the more positive redox potential of the Ni^{2+}/Ni ($E^\circ = -0.23$ V) pair compared to the conduction band of TiO_2 ($E^\circ = -0.26$ V) which served as active sites for the reduction of H^+ to H_2 (Fig. 20).[231] In another study, it is postulated that $Ni(OH)_2$ is converted to NiO after prolonged irradiation in the oxidizing environment of the reaction mixture.[117] There is some controversy in the literature about the valence and conduction band energies of NiO.[232] Values in the range of −0.3 to −1.0 eV are reported for the conduction band and 2.4 to 4.3 eV for the valence band (with respect to SHE).[233] Thus, NiO cannot capture photogenerated electrons from the conduction band of TiO_2 because the conduction band of NiO is more negative than that of TiO_2. However, theoretical calculations show that H:H recombination on NiO(100) is exothermic, with an activation barrier of only 40 kJ mol^{-1}.[234] The high hydrogen production rates observed on NiO/TiO_2-containing catalysts can be explained by the ability of NiO to act as a site for recombination of adsorbed atomic hydrogen after H^+ has accepted an electron directly from the conduction band of TiO_2.[117]

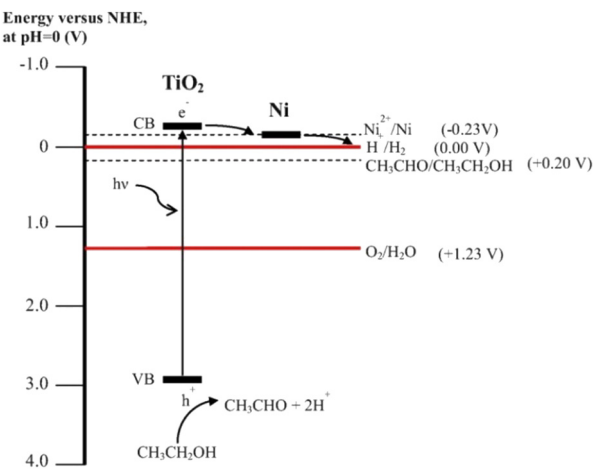

Fig. 20 Schematic illustration of important electron transfer processes in the Ni/TiO_2 system leading to H_2 production. Reprinted with permission from Elsevier.[231]

Fujita and co-workers reported that the loading of p-type NiO over n-type TiO_2 conductors produces a p–n heterojunction, which generates an internal electric field at the NiO/TiO_2 interface.[235] It was proposed that this field accelerates electron transfer for proton reduction at the NiO, thus strongly suppressing the recombination of photogenerated electrons and holes. With reference to some studies it was found that highly dispersed and exclusively metallic Ni particles are excellent hydrogen production sites.[231] Recently, the hydrogen production activity of a series of Ni/TiO_2 photocatalysts in ethanol–water mixtures was investigated.[236] It was found that the photocatalytic activity of Ni/TiO_2 photocatalysts strongly depends on the Ni zero oxidation state and loading, with a loading of 0.5 wt% is optimal, giving a hydrogen production rate of 24.3 mmol h^{-1} g^{-1} in 95 vol% aqueous ethanol under a UV flux equivalent to sunlight (about 4–5 mW cm^{-2}). This high activity of the Ni/TiO_2 photocatalyst was attributed to the Fermi level of Ni^0, which is positive with respect to the conduction band of TiO_2 and negative with respect to the H_2O/H_2 redox couple. The high work function of nickel is also advantageous in preventing the back migration of electrons, since an excellent Schottky junction formed at this interface. In the same work, 0.63 wt% NiO/TiO_2 was tested. A long induction period observed before a constant hydrogen production rate was reached, which was about a quarter of that of Ni/TiO_2. This induction period was explained by the *in situ* reduction of part of the NiO to Ni^0 by the hydrogen produced in the initial phase of the reaction. The Fermi level of Ni^0 is below that of the conduction band of TiO_2 anatase.

Bimetallic TiO_2

Bimetallic heterogeneous catalysts are widely employed in many fields of catalysis, due to high performances; increased activity and selectivity to desired products, extended lifetime arising from the cooperative interactions between the two metals.[237–247] Heterojunction is formed when two different materials with varied work functions (or electron affinity) are in electrical contact with each other. The surface energy of the metal and combined metals, dissociation energy, standard reduction potential, bond enthalpies, miscibility, metal–metal and metal–TiO_2 lattice interactions, and reduction kinetics of the metals results in the various configurations:[243] (1) distribution of

both the metals over the TiO_2 surface; (2) core–shell structure of the metals decorated over the TiO_2 (and *vice versa*) and (3) alloy-like structure dispersed over the TiO_2. The type (3) enables the effective interaction of both the metals with one another as well as with TiO_2. Type (2) provides suitable platform for metal–metal interactions and that the metallic core may not have substantial interactions with titania. The induced internal electric field at the interface between the metal–metal and metal–titania redistributes the charge density and charge carriers drift directionally along the electric field force.[243] However, direction of electron transfer between the interface metal atoms is difficult to determine owing to the different bonding environments, and bonding situation at the interface is very complex because of shorter interfacial spacing and multiple layers of atoms.[243]

It is well known that the work function of a given metal decreases by alloying with other metal with a lower work function. This suggests that alloying of other metal with Pt would decrease the work function of Pt nanoparticles, Pt is having highest work function among noble metals. This may raise Fermi level potential of metal and promote efficient electron transfer from TiO_2 to metal nanoparticles. The bi-metallic deposited TiO_2 may exhibits some unique characteristics properties which are different than that of mono metallic due to the synergistic effect between the monometallic counterparts. For example, when the Pt–Cu co-modified TiO_2 is used as a photocatalyst, nitrate can be selectively reduced to N_2 under irradiation. In contrast, nitrate is mainly converted to ammonia or nitrite over the Pt modified TiO_2 or the Cu modified TiO_2, respectively.[248] Similarly, highly selective ammonia synthesis from nitrate can be observed in the presence of the Pd–Cu co-modified TiO_2 while only as small amount of NO_3^- is converted to ammonia in the presence of the Pd-modified TiO_2.[249] The use of bimetallic catalysts for hydrogen production through photo-reforming has started very recently. Only a few bimetallic systems, namely Au/Pd core–shell nanoparticles,[177,250] Au/Pt Nano-alloys[251–253] immobilized on TiO_2 and polymer protected Pt/Ru bimetallic clusters[254] have been investigated for H_2 production. The structure of bimetallic nanoparticles can range from core–shell (cherry) structures to bimetallic hetero-structures, (nano) alloys, intermetallic *etc.*, as shown in Fig. 21.

Au–Pt nano-alloys/TiO_2. Bimetallic Au–Pt systems are widely employed as traditional heterogeneous catalysts and show evidence of electronic transfers from Au to Pt.[257] Santo and co-workers studied the effect of Au–Pt bimetallic nanoparticles loaded on TiO_2 and the structural modification of the support (TiO_2) in the photo-reforming of ethanol and glycerol.[251,252] Bimetallic 0.5 wt% Au–0.5 wt% Pt/TiO_2 catalyst showed good hydrogen production rate both under simulated visible light and UV-A light from ethanol–water mixtures. The higher activity of Au–Pt/TiO_2 catalyst was ascribed to the positive synergistic interaction between the Au and Pt. These interactions can induce a decrease in the metal–hydrogen bond strength (*i.e.* easier desorption of H_2 from the metal surface), and improve the electron trapping ability of the nanoparticles. However, these studies were carried out at higher noble metal loading (1 wt%) and for only one Au–Pt ratio (1 : 1). Later on Pedro and co-workers provided further information to establish the optimal metal amount and proportion between Pt and Au.[253] In their work the photocatalytic photo-reforming of Au–Pt Nano-alloys, deposited on P25 TiO_2 was compared under UV, visible and simulated solar light irradiation, both in the presence and absence of methanol as a sacrificial electron donor. When UV light was used for excitation, photons were mainly absorbed by TiO_2 and then the presence of a large percentage of Pt in the Nano-alloy was beneficial because it accelerates hydrogen evolution through fast proton reduction. In contrast, when using exclusively visible light, photons ware absorbed by Au nanoparticles and in this case, the presence of Pt was detrimental when hydrogen evolution is not the controlling step. Under simulated sunlight the situation was balanced between visible light absorption and faster hydrogen evolution by the presence of optimal Au and Pt content in the Nano-alloy. Optimum loading of both the metals was 0.25 wt% in each case, with most active photo-catalysts containing, 70–100% Pt in UV, 80–100% Au in visible and 78%Au–22%Pt in the simulated solar irradiations.

Au–Pd/TiO_2. Au–Pd (3/1) Nano-alloy deposited over TiO_2 was recently studied for the hydrogen production from photo-reforming of formic acid. Higher hydrogen yield in this reaction was attributed to good electron sink effect by Au–Pd Nano-alloy and surface Plasmon mechanism by higher amount of gold.[258] Idriss and co-workers studied hydrogen production over Au–Pd (1/3) alloy/TiO_2 system through photo-reforming of ethanol, an higher activity of catalyst was again attributed to the surface Plasmon effect shown by lager gold particles and efficient electron trapping of smaller Pd nanoparticles.[259] Masahashi and co-workers reported H_2 evolution from the photo-reforming of ethanol aqueous solution using core–shell Au/Pd (different molar ratio: 0/1, 1/3, 1/1, 3/1, 1/0) bimetallic nanoparticles immobilized on TiO_2 support by sonochemical method.[250] The improved photocatalytic activity was attributed to inhomogeneous distribution of electrons due to selective H_2 permeability by the Pd–shell which might contribute to the selective donation of photogenerated electrons to protons and localization of electrons in the Au–core. Previously, a blue shift in the Au Plasmon absorption peak was observed in the spectra of the aqueous dispersion containing Au_{core}/Pd_{shell} bimetallic nanoparticles, indicating that the electron density in the Au–core had increased and the Pd–shell possessed a relative positive charge.[260] However, Masahashi and co-workers neither considered the electronic properties of nanoparticles elemental configurations, which would be important for understanding

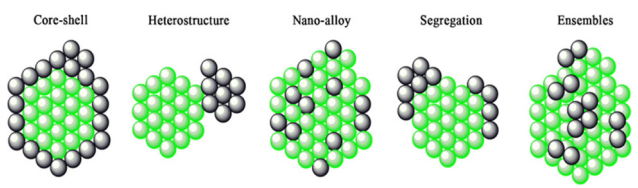

Fig. 21 A pictorial representation of bimetallic nanoparticles structures. Reproduced with permission from John Wiley and Sons.[255,256]

the ability to trap photoexcited electrons and effects on photocatalytic performance, nor the natural alignment of electron levels in nanoparticles with the band structure of a semiconducting substrate, which would provide insight into the favorability of the transfer of photoexcited electrons from the substrate to the nanoparticles. Su and co-workers optimized the electronic properties of Au and Pd cocatalyst in bimetallic nanoparticles to enhance the photo-reforming of many polyoxygenated compounds.[177] They showed that that fine tuning the Au–Pd nanoparticle structure over TiO_2 modified the electronic properties of the cocatalyst significantly. Density functional theory (DFT) was applied to gain insight into how the morphology and the elemental distribution of the nanoparticles alter the electronic properties. The extracted density of states (DOS) for icosahedral Au and icosahedral Pd clusters (Fig. 22a and b) reveal that many more unoccupied states lay just above TiO_2 Fermi level ((E_F)) in the case of the icosahedral Pd cluster, which would be favorable for the trapping of electrons and performing redox reactions. The natural alignment of the nanoparticles DOS with the conduction band for TiO_2 shows that photoexcited electrons would energetically transfer to the metallic nanoparticles, as the E_F of the nanoparticles lies below the conduction band minimum (CBM) of TiO_2.[261] Moreover, for the bimetallic core–shell structures, the number of unoccupied surface states just above the E_F increases with surface Pd concentration.[261]

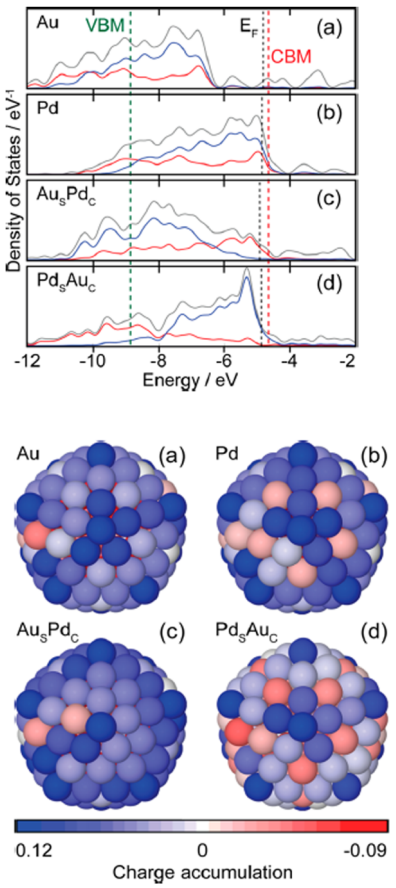

Fig. 22 (a–d) Electronic density of states (DOS) profiles of 147-atom icosahedral clusters of Au, Pd, Au_sPd_c, and Pd_sAu_c, respectively. The total valence DOS (gray) is complemented by the contributions of the d-orbitals in both the core (red) and outer shell (blue) region. E_F of the metal clusters, conduction band minima (CBM), and valence band maxima (VBM) of TiO_2 are indicated by black and red dashed lines, respectively.[261] 27B (a–d) Charge localization from the view of the (100) surface of 147-atom icosahedral clusters of Au, Pd, Au_sPd_c, and Pd_sAu_c, respectively. The blue and red colors represent atoms with electron accumulation and depletion, respectively. Reprinted with permission from American Chemical Society.[177]

Cu–Ni/TiO_2. The previous results confirmed that Cu is a promising alternative to Pt in this photocatalytic system.[262,263] Considering that Ni is also an efficient co-catalyst in some photocatalysts,[264,265] it can be inferred that the bimetallic Cu–Ni co-catalyst could have high reactivity in the TiO_2-based photocatalytic system due to a synergistic effect. It is still unclear whether the TiO_2 nanoparticles co-modified with Cu and Ni are an efficient photocatalytic system or not. Tian and co-workers synthesized Ni–Cu co-modified TiO_2 by a simple hydrothermal method for hydrogen production from a methanol–water system.[266] The formation of Cu–Ni alloy was confirmed by HRTEM and XPS analyzes, along with the formation of a layer of $Ni(OH)_2$ covering the Cu–Ni alloy. Upon irradiation with UV light, $Ni(OH)_2$ was further reduced to Ni(0) as the Cu–Ni alloy transfers an electron to $Ni(OH)_2$, forming Cu–Ni@Ni, which can serve as a better cathodic site for electron transfer.

The work functions of Cu and Ni are 4.94 eV[268] and 5.15 eV,[269] respectively, and the work function of bimetallic Cu–Ni is at the level between Cu and Ni. As a result, a more appropriate height of Schottky barrier was obtained between TiO_2 and Cu/Ni alloy than between TiO_2 and the single metal. Recently, our group has prepared bimetallic Cu/Ni hydroxide-supported TiO_2 photocatalysts for hydrogen production from alcohol–water mixtures. The mechanism of hydrogen production *via* Cu/Ni hydroxide supported TiO_2 has been discussed in detail. It was proved that $Cu(OH)_2$ is reduced to metallic Cu by the conduction band electrons of TiO_2 due to a suitable redox potential, but $Ni(OH)_2$ cannot be directly reduced by the conduction band electrons of TiO_2. Thus, when the pH of the reaction mixture falls to 4 after one hour of photoreaction, the $Ni(OH)_2$ dissolves as free Ni^{2+} ions, which can now be thermodynamically reduced by the conduction band electrons of TiO_2 to metallic Ni and deposited as a separate proton reduction site or *via* electron-rich Cu to form a Cu/Ni alloy (Fig. 23).[267] The stability of these systems is a crucial issue that requires adequate understanding. Long-term performance needs to be assessed even though no one has reported any stability issues. Since strongly reducing conditions preserve the metal in its metallic state and keep it stable under photoreaction conditions, it is commonly accepted that non-Nobel metals are stable systems.[226,227,264,265,267]

Metal loading methods

Metal loaded photocatalysts are usually prepared using photodeposition,[139,270] impregnation,[13,271,272] photoreduction and

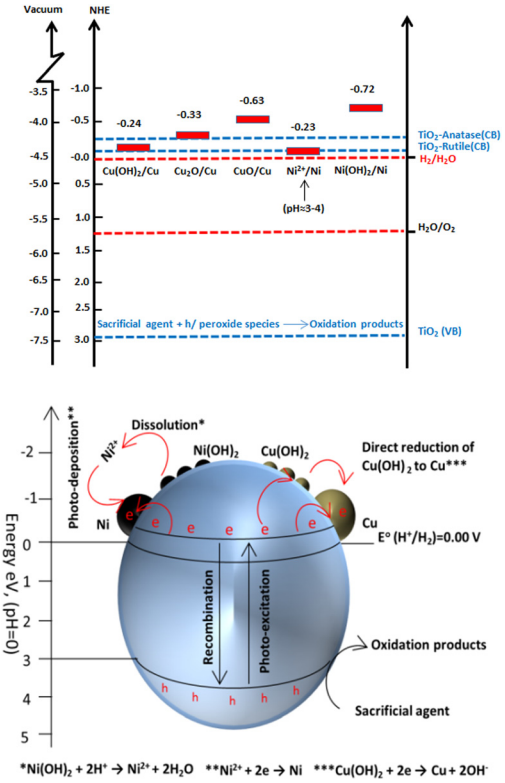

Fig. 23 Schematic illustration for hydrogen production, charge transfer, separation and chemical conversions in $Ni(OH)_2$ and $Cu(OH)_2$ nanoclusters modified TiO_2 system under photoreaction conditions. Reprinted with permission from John Wiley and Sons.[267]

chemical reduction with H_2 or $NaBH_4$.[139,270,273] Photodeposition method is most widely used to load due to its easy handleability, high-efficiency and repeatability and in most cases this method yields more active photocatalyst.[274,275] This is in line with the rational that metal is preferentially deposited on semiconductor sites with high electron density under photoreaction conditions. On the other hand the impregnation method includes impregnation of TiO_2 with the Pt precursor solution, drying, and finally reduction at *ca.* 500 °C.[135,276] Although this method is simple, easily manipulated and all of the metal in the solution is used but results in lower activity due to greater particle size.[277] Other methods including sonochemical reduction method by prolonged sonication,[278] plasma-enhanced impregnation method to improve the dispersion of Pt, modified conventional impregnation method by utilizing glow discharge plasma,[136] have also been employed.

Photocatalysis by supported single metal atom

As was previously discussed, cocatalysts, particularly noble metal particles, are important to be deposited onto semiconductors in order to improve charge separation and modify the kinetics of surface reactions.[8,279] However, the low exposed number of metal atoms and the weak interaction between the metal and support significantly restrict the catalytic activity of particle-based cocatalyst systems. Since only the atoms on the surface of metal particles are involved in catalytic processes,[11] reducing the size of metal particles to a single atom is an efficient way to get around this problem.[280–282] Furthermore, since metal atoms act as the catalytic centres, improving the loading density of individual metal atoms will improve catalytic performance even further (Fig. 24). In addition, single atom photocatalysis offers the following intriguing advantages over its bulk, nanoparticle, and nanocluster equivalents: (i) Due to their unique electronic structures and unsaturated coordination centers, they exhibit high activity and selectivity;[283,284] (ii) a significant decrease in the use for catalytic metals;[285,286] (iii) simple to understand reaction mechanisms due to single-atom reactive sites;[287,288] and (iv) an excellent platform to understand the structure–performance correlation based on their atomic-level structures.[289,290]

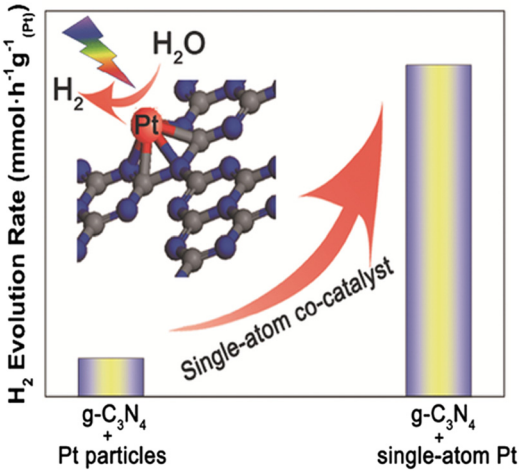

Fig. 24 The highly stable single-atom co-catalyst (Pt) embedded in the sub-nanoporosity of 2D g-C_3N_4 leading to significantly enhanced photocatalytic H_2 evolution activity. Reprinted with permission from John Wiley and Sons.[286]

The creation of an effective approach to stabilize the loading of high density metal atoms on the support photocatalyst is the key. The stability of single-atom photocatalysts depends on interactions between the metal and the support. In these interactions, the metal atoms are often stabilized by nearby surface atoms or ligands on the support, preventing their diffusion and aggregation.[291] Strengthening the impact of the metal–support interaction on single-atom photocatalysts is a common approach for designing and producing single-atom-based photocatalysts.[292] This is typically accomplished through the modification of the supporting materials, such as anchoring surface sites (defects and vacancies), heteroatom doping, coordinating with organic bridging ligands, and anchoring on metal–organic frameworks.[291]

Therefore, before using the support in photocatalytic reactions, it is important to choose and modify it. There has only been few studies where Single atom supported semiconductors have shown improved performance for H_2 production

from photoreforming of organics. Given its potential and advantages over conventional metal-supported photocatalysts, we anticipate that this system will have a high potential for photoreforming applications because of its inherent advantages as discussed above. It may also contribute to an increase in activities to the point where they are sufficient to support industrial scale applications.

Role of surface face

It is well known that anatase (001) facet is more active than (101) and (100) facet because of its higher surface energy and is more reactive for dissociation of water molecules.[293–301] Surface hole stability trends in rutile and anatase are (100) < (110) < (011) < (001) and (011) < (100) < (001) respectively.[293–301] Surface hole trapping levels of TiO_2 with the exception of (100) rutile are well above the valence band edge (3.0 V [NHE]) and thus stabilized (less reactive). For instance a hole stabilization on anatase (001) of 1.3 eV reduces the oxidative power to *ca.* 1.7 V [NHE]. But at the same time this hole stability with respect to the bulk value is a large driving force for hole transport to the surface and enhances the equilibrium surface hole density by 10^{20} at room temperature.[302] The hole diffusivity of anatase TiO_2 at room temperature is known to be about 4×10^{-5} m^2 s^{-1}.[303] Based on these results, it is believed that the fast hole decay process mostly reflects the trapping of holes that are excited near the surface. While the slow decay process corresponds to trapping and/or recombination processes of the holes that are excited inside the particle. Yu and co-workers performed Pt loading on fluorinated anatase nanosheets with 75% exposed (001) facets by photochemical reduction deposition method. Surface fluorination was useful to stabilize the high energy (001) facets. A very good rate of hydrogen production was observed by the synergistic effect of surface fluorination, exposed (001) facets and Pt loading.[304] The experimental results and density functional theory calculations reveal that holes and electrons tend to reach and react at the same surface sites, *i.e.*, crystal edge/corner, owing to the exposed (001) and (101) facets of TiO_2.[305] These findings offer insights into the nature of photocatalytic active sites and imply an activity-based strategy for rationally engineering catalysts for improved photocatalysis, which could be also applied for other catalytic materials.

Dye sensitized TiO_2

Another method to boost activity in the visible range is to sensitize metal-supported TiO_2 using dyes.[306] The most important criteria when choosing a dye is to make sure that it will not be photooxidized by TiO_2.[11] The various steps for producing H_2 on such systems are depicted in Fig. 25. In the H_2 photocatalytic production, a number of rationally designed donor–acceptor dyes can be utilized as sensitizers. The reaction process, the way dye interacts with organic materials, and the structural and electrochemical characteristics of the sensitizers all affect the rate of H_2 generation. The photocatalytic process may be

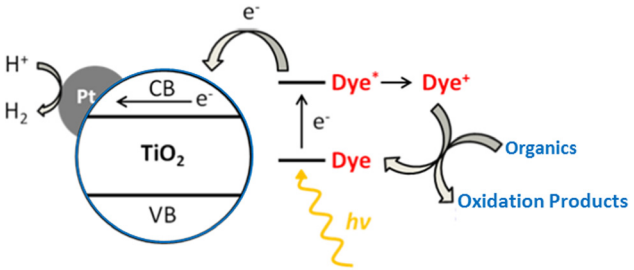

Fig. 25 Schematic illustration for hydrogen production, on dye sensitized Pt/TiO_2 system under photoreaction conditions. Reproduced with permission from John Wiley and Sons.[306]

hampered by charge recombination between injected electrons in TiO_2 and the oxidized dye if dye regeneration is slower, based on the molecular structure and electronic characteristics of the dyes.[307,308]

Therefore, an increase in electron density on TiO_2 can aid increase hydrogen generation rates by boosting light harvesting efficiency in conjunction with a greater driving force for electron injection. Accordingly, in order to provide the best results, the molecular design of sensitizers should be carefully adjusted based on the specific organic (and set of conditions) employed in the experiments. A breakthrough in dye-sensitized photocatalytic H_2 production sustainability may result from precisely calibrated sensitizers, broadening the spectrum to a variety of organics and perhaps biomass-derived feedstocks.[307,308] Dibranched donor–(π–acceptor)$_2$ dyes have been investigated as photosensitizers in the photocatalytic production of H_2 in conjunction with a Pt/TiO_2 catalyst. Phenothiazine, cyanoacrylic acid and mono-/poly-cyclic fused thiophene π derivatives serve as donor core, acceptor/anchoring group and light harvesters, respectively. The dyes optical and electrochemical characteristics can be improved by carefully designing thiophene-based spacers. These thiophene-based sensitizers show increased stability after longer irradiation times and improved performances in terms of H_2 production rates and light-to-fuel efficiencies.[309,310]

Au/TiO_2 superstructures

One of the most difficult missions is to find suitable materials as photocatalysts that can not only harvest the full spectrum of solar light, from ultraviolet to near-infrared (NIR) region, but also achieve high and efficient solar-to-hydrogen conversion. Catalysts and effective optoelectronic devices have been developed using metal–semiconductor nanocomposites. These performance of such nanocomposites is greatly impacted by the electrical and morphological properties of the metals and semiconductors they are made of. Novel nanocomposites containing plate-like anatase TiO_2 mesocrystal superstructures and noble metal (Au, Pt) nanoparticles preferentially photodeposited on the edge of TiO_2 mesocrystals have been prepared. The findings showed that the majority of photogenerated electrons could move from the dominant surface to the edge of the TiO_2

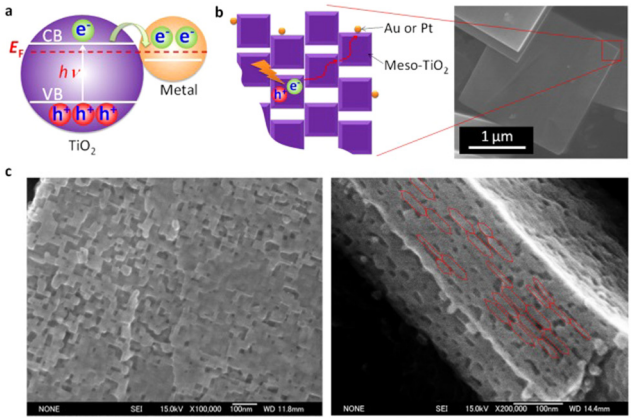

Fig. 26 Diagrammatic representation of (a) electron transfer from noble metal (Au, Pt) nanoparticles to TiO_2 upon UV light exposure. (b) The transfer of electrons on Au or Pt/*meso*-TiO_2. *Meso*-TiO_2 is constituted of an orderly alignment of anatase TiO_2 nanocrystals, as shown in the SEM picture in panel b. *Meso*-TiO_2 typically has dimensions of 2–5 um and a thickness of 50–300 nm. (c) SEM pictures of the *Meso*-TiO_2 basal (left) and lateral (right) surfaces. Reprinted with permission from American Chemical Society.[311]

mesocrystal, with reduction reactions primarily taking place at {101} facets (Fig. 26). This allowed for a significant (more than one order of magnitude) increase in the photocatalytic reaction rate in organic degradation reactions. The charge recombination of these electrons with the holes in the Au NPs is greatly inhibited by this anisotropic electron flow, increasing the visible-light photocatalytic activity. Compared to conventional TiO_2 nanocrystal samples, these exceptional characteristics considerably minimize the amount of Au or Pt loading on the TiO_2 mesocrystal while maintaining the same photocatalytic activity.[311,312]

Au nanosphere, mono-encapsulated in TiO_2 hollow nanosphere, and three-dimensionally assembled array of these Au–TiO_2 show multiscattering effect and exhibit a significantly higher photocatalytic activity of H_2 generation than Au–TiO_2 (3.5 folds under visible light irradiation and 1.4 folds under solar light irradiation). The longer light path length caused by multiscattering between Au–TiO_2 and reflection inside the TiO_2 shell accounts for the 3D-increased array's activity. As a result, the nanosphere has a greater chance to absorb light, and more hot electrons are anticipated to be produced by the electron transfer from the Au nanosphere to the TiO_2 shell, increasing the formation of H_2.[313] A wide solar response photocatalyst was developed employing Au/$La_2Ti_2O_7$ sensitized with black phosphorus, and optimum H_2 generation rates of around 0.74 and 0.30 mmol g^{-1} h^{-1} at wavelengths longer than 420 nm and 780 nm, respectively, have been reported. The increased photocatalytic activity in the visible and NIR light ranges is a result of the extensive absorption by black phosphorus and plasmonic Au. It was proposed that the strong photoactivities found were caused by the effective interfacial electron transport from excited black phosphorus and Au to $La_2Ti_2O_7$.[314] The above-mentioned outcomes offer us a new viewpoint on building structures that effectively utilize light and considerably enhance photocatalytic activities due to their unique structure as compared to conventional photocatalytic materials.

Catalyst benchmarking

Although the focus of this review is on the qualitative effects of different factors on photoreforming, it is crucial to talk about how important it is to describe the results in photocatalysis with clarity. A catalyst's activity is often measured in terms of the amount of reaction happened over a certain period of time per unit of catalyst material (weight, surface area, or volume), turnover frequency (TOF), apparent quantum yield (AQY), and solar to hydrogen (STH) efficiency. Due to its specificity to pure water splitting, STH is perhaps the most crucial metric yet is frequently reported inaccurately for reactions including sacrificial agents.

Reporting rates of product generated by the total mass of catalyst is a typical practice in trying to define the benefits of photocatalysts. An analysis of the catalyst activity may be erroneous as a result of this prevalent practice of reporting activity. By measuring the rate over the catalyst's surface area, it is possible to demonstrate that the enhancement of activity seen in reporting reaction rate per unit mass, particularly for multicomponent catalysts, may in fact be due to simple geometric factors. When normalized by mass, it was discovered in a research of Au/TiO_2 photocatalysts for H_2 evolution that the micro- and nanostructured catalysts showed a substantial variation in activity.[315] We recommend authors to include both data reporting processes. Although this does not completely eliminate all the variables that could affect the actual catalysis (since not all of the surface is guaranteed to be illuminated, the surface area should also be combined with a complete morphological analysis of the material porosity), we think it would be a more reliable way to report activity. Surface area normalization, on the other hand, has a more academic sense.

In fact, part of the potentially active surface during photocatalytic tests is not illuminated due to shading (scattering and reflection), not participating in the catalysis. Therefore, the efficiency must be somehow connected to the percentage of light that the catalyst actually uses. Due to this, the term apparent quantum yield (AQY), which describes the quantity of incident photons of a specific wavelength per unit of time and volume that enter the photoreactor, has been developed.[316] Recently, models that can better accommodate more complex photocatalytic materials, including heterojunctions, were presented. These models allow the QY (or AQY) to be derived from reaction rates under simulated solar or polychromatic light.[317] If monochromatic light is utilized for the AQY evaluation, the wavelength selection must be as compatible as possible with the optical characteristics of the photocatalyst.[318] Reporting the AQY determined with a single monochromatic light source may be deceptive if the catalyst can absorb light of various wavelengths. Last but not least, the as-calculated quantum yield should include all experimental information in addition to the wavelength used, such as the reactor's shape and the precise

length of the catalytic experiments on which the number of moles of product and the number of photons were counted; the latter is important because the rate of product formation might not be constant over time.

In recent publications, comparison tables featuring cutting-edge catalysts are showing up more frequently. If you choose them carefully, rationally, and fairly, they will be more beneficial. These tables should compare as many performance parameters as possible, not just one. The stability and selectivity of the catalyst, two equally significant parameters of comparison, cannot be fully understood by reporting merely a comparison of quantum yields. Since the period of the experiment is chosen arbitrarily for the purpose of calculating the yield, it is easy for the authors to influence it for their own convenience and lose impartiality, especially when the rates of product production are not constant. Additionally, a catalyst with a higher QY or AQY may only be artificially superior because it does not exclude the possibility that other unobserved mechanisms contributed to the developed product (parallel experiments in the dark under same conditions of temperature, catalyst loading, *etc.* must be invariably carried out).[319]

Conclusions and future work

There is debate on whether the metals act as electron sink and H recombination center or recombination center alone.[117,315] Regardless it is important to prepare extremely small metal particles (high dispersion) to increase the photo-reforming rate per gram of catalyst. Strategies to produce metal single-atom catalysts in the heterogeneous catalysis field can be adopted and utilized. In general, the rate of H_2 production increases with an increase in metal loading. The maximum amount of H_2 production is observed in metal% loading between 1.5–3 wt%.[11,279,315] Beyond this loading, a decrease is observed. This decrease is often ascribed to the metal shadowing effect. Keeping this in mind, a catalyst with metal nanoparticles containing only a few atoms and uniformly distributed on the surface seems the way to go. However, it is very difficult to prepare the high dispersed metal catalysts. There are few studies in which appropriate metal particle sizes were carried. Puskelova and co-workers synthesized highly porous TiO_2–Pt aerogel composites by mixing sol–gel synthesized TiO_2 with Pt colloidal suspension followed by supercritical drying and subsequently annealing at 500 °C. Metal particle size was tuned by adding tri-sodium citrate. The hydrogen production rate was enhanced due to more reactive Pt sites of smaller tunable particles and higher support surface area.[320] Recently Naldoni and co-workers demonstrated that adsorption of metal particles followed by the reduction with $NaBH_4$ was a superior method than others to develop intimate contact and a very fine degree of dispersion.[129] Li and co-workers prepared visible light active photocatalyst by mixing Pt/TiO_2 with luminescence material Er^{3+}:$Y_3Al_5O_{12}$ which can absorb visible and infrared light in solar spectrum and emit ultraviolet light to fulfill the requirements of TiO_2 for water reduction. This technique may provide an effective way of harvesting solar energy for large scale hydrogen production in future.[321–324] Further work must be conducted on improvements in the efficient and affordable preparation of single atom supported semiconductors. For instance, it can offer the much more catalytic sites possible while also limiting the shadowing effect among other advantageous qualities as previously discussed.

Among all the catalysts studied for photoreforming so far, TiO_2 offers more advantages in terms of industrial applications than any other catalyst. However, TiO_2 can absorb only less than 5% of sunlight because of its wide band-gap. Various strategies, the most prominent of which is TiO_2 doping have long been researched as almost all the dopant help to increase visible light absorption. However, there is not much promise in this strategy because dopants are detrimental to photoreforming rates as they create defects that act as recombination centers. Li and co-workers prepared visible light active photocatalyst by mixing Pt/TiO_2 with luminescence material Er^{3+}:$Y_3Al_5O_{12}$ which can absorb visible and infrared light in the solar spectrum and emit ultraviolet light to fulfil the requirements of TiO_2 for water reduction. This technique may provide an effective way of harvesting solar energy for large-scale hydrogen production in the future.[185,321–323] Since black TiO_2 not only absorbs photons across a wide spectral range (UV to IR region), but also modifies the structural and morphological features, along with the electronic properties of the material, significantly improving the catalytic performance, the associated drawbacks of white TiO_2 and its modified forms were addressed to a large extent after its discovery.[325] The synthesis procedures required, though, are laborious and challenging. With increased knowledge of its electronic structure and stability under reaction conditions, additional research with the goal of producing black TiO_2 under milder, less energy-intensive conditions may help further improve its activity.[326]

It appears that H_2 production using TiO_2 based catalyst has reached its plateau and there is only a marginal increase in rates. Further work needs to be focused more on fundamental understanding using state-of-the-art facilities that bring progressive improvement in capabilities. Electron–hole recombination is a critical problem that has, so far, limited the efficiency of the most promising photocatalytic materials. Apart from metal, the electron–hole recombination can be reduced by carefully designing the geometrical structure of semiconductor particles to allow anisotropic migration of electrons and holes. For, example, H_2 production from alcohols in uniform, one-dimensional brookite TiO_2 nanorods is highly enhanced by engineering their length. The hole and electron diffusion lengths in TiO_2 are about 10 nm and several micrometers, respectively.[327] The holes are effectively confined to the width of the nanorods, whereas electrons are free to move over the whole length, due to their 1D nature.[328] For these reasons, the high H_2 production rate of the long rods with the delocalization of electrons along their 1D structure, favors electron−hole separation and carrier extraction by protons and the alcohol.[329] Chong and co-workers recently reported hydrogen production by Cu doped TiO_2 films with preferred (001) orientation by the RF magnetron

sputtering method.[330] They concluded that Cu dopant not only induced the slight transformation of anatase to rutile phase but was also useful to synthesize TiO_2 films with preferred high energy (001) facets.[331] Water molecules can easily dissociate on the (001) facet which will enhance the transfer of photogenerated charge carriers from films to water molecules.[332–334] Cu(I) species can effectively prevent the recombination of charge carriers by trapping the photogenerated electrons. Further investigations in this direction are needed, that may be help to enhance overall photcatalytic activity in synergy with loaded metals.

Even after decades of research on TiO_2, water oxidation reaction kinetics has not been improved. There is a need to understand why the kinetics of water oxidation is slow although this reaction is thermodynamically more favorable as compared to its reduction. Studies focused on water oxidation reaction understanding may provide answers. Recently Idriss and co-workers studied the water oxidation reaction using cerium(IV) cations as sacrificial agents using Ir/TiO_2 catalyst.[335] More similar works are needed to understand the kinetics and thus enhance the reaction rates. Further investigation of photonic crystals can help enhance the H_2 production from photo-reforming. At the moment the work is at its initial stages and suffers from low activities mainly due to the impurities added into the structure during the preparation of photonic crystals. Further TiO_2 photonic crystals have defect states that need to be eliminated without destroying photonic crystals structure. These impurities decrease the activity considerably by providing e–h recombination centers.[169,170]

Author contributions

All the authors contributed in writing this manuscript. The corresponding author conceptualized and supervised writing of the manuscript.

Conflicts of interest

There are no conflicts to declare.

Acknowledgements

The authors of this work acknowledge the resource support from all the institutions listed under author(s) affiliation.

References

1 M. Ni, M. K. H. Leung, D. Y. C. Leung and K. Sumathy, *Renewable Sustainable Energy Rev.*, 2007, **11**, 401–425.
2 J. Schneider, M. Matsuoka, M. Takeuchi, J. Zhang, Y. Horiuchi, M. Anpo and D. W. Bahnemann, *Chem. Rev.*, 2014, **114**, 9919–9986.
3 N. Rahimi, R. A. Pax and E. M. Gray, *Prog. Solid State Chem.*, 2016, **44**, 86–105.
4 A. J. Haider, Z. N. Jameel and I. H. M. Al-Hussaini, *Energy Proc.*, 2019, **157**, 17–29.
5 M. T. Noman, M. A. Ashraf and A. Ali, *Environ. Sci. Pollut. Res.*, 2019, **26**, 3262–3291.
6 C. Y. Toe, C. Tsounis, J. Zhang, H. Masood, D. Gunawan, J. Scott and R. Amal, *Energy Environ. Sci.*, 2021, **14**, 1140–1175.
7 S. Banerjee, J. Gopal and P. Muraleedharan, *et al.*, *Curr. Sci.*, 2006, **90**, 1378–1383.
8 A. K. Wahab, M. A. Nadeem and H. Idriss, *Front. Chem.*, 2019, **7**, 780.
9 M. A. Nadeem, K. A. Connelly and H. Idriss, *Int. J. Nanotechnol.*, 2012, **9**, 121–162.
10 A. V. Puga, *Coord. Chem. Rev.*, 2016, **315**, 1–66.
11 M. A. Nadeem, K. A. Connelly and H. Idriss, *Int. J. Nanotechnol.*, 2012, **9**, 121–162.
12 Y. Xu and M. A. A. Schoonen, *Am. Mineral.*, 2000, **85**, 543–556.
13 N.-L. Wu, M.-S. Lee, Z.-J. Pon and J.-Z. Hsu, *J. Photochem. Photobiol., A*, 2004, **163**, 277–280.
14 A. Nuhu, J. Soares, M. Gonzalez-Herrera, A. Watts, G. Hussein and M. Bowker, *Top Catal.*, 2007, **44**, 293–297.
15 T. Bak, J. Nowotny, M. Rekas and C. C. Sorrell, *Int. J. Hydrogen Energy*, 2002, **27**, 991–1022.
16 A. Kudo, *Pure Appl. Chem.*, 2007, **79**, 1917–1927.
17 M. Koelsch, S. Cassaignon, C. Ta Thanh Minh, J. F. Guillemoles and J. P. Jolivet, *Thin Solid Films*, 2004, **451–452**, 86–92.
18 A. Amtout and R. Leonelli, *Phys. Rev. B: Condens. Matter Mater. Phys.*, 1995, **51**, 6842–6851.
19 R. Asahi, Y. Taga, W. Mannstadt and A. J. Freeman, *Phys. Rev. B: Condens. Matter Mater. Phys.*, 2000, **61**, 7459–7465.
20 W. Wunderlich, T. Oekermann and L. Miao, *et al.*, *J. Ceram. Process Res.*, 2004, **5**, 343–354.
21 M. Rao, K. Rajeshwar, V. P. Verneker and J. DuBow, *J. Phys. Chem.*, 1980, **84**, 1987–1991.
22 K. Lalitha, J. K. Reddy, M. V. Phanikrishna Sharma, V. D. Kumari and M. Subrahmanyam, *Int. J. Hydrogen Energy*, 2010, **35**, 3991–4001.
23 H. Idriss, *Curr. Opin. Chem. Eng.*, 2020, **29**, 74–82.
24 D. Chatterjee and S. Dasgupta, *J. Photochem. Photobiol., C*, 2005, **6**, 186–205.
25 E. Kowalska, R. Abe and B. Ohtani, *Chem. Commun.*, 2009, 241–243.
26 A. J. Bard and M. A. Fox, *Acc. Chem. Res.*, 1995, **28**, 141–145.
27 R. Baba, S. Nakabayashi, A. Fujishima and K. Honda, *J. Phys. Chem.*, 1985, **89**, 1902–1905.
28 A. Henglein, *Chem. Rev.*, 1989, **89**, 1861–1873.
29 J. Z. Zhang, *Acc. Chem. Res.*, 1997, **30**, 423–429.
30 K. G. Thomas and P. V. Kamat, *Acc. Chem. Res.*, 2003, **36**, 888–898.
31 P. V. Kamat and D. Meisel, *Curr. Opin. Colloid Interface Sci.*, 2002, **7**, 282–287.
32 W. Choi, A. Termin and M. R. Hoffmann, *J. Phys. Chem.*, 1994, **98**, 13669–13679.
33 M. A. Nadeem, G. I. N. Waterhouse and H. Idriss, *Surf. Sci.*, 2016, **650**, 40–50.

34 C. Young, T. M. Lim, K. Chiang, J. Scott and R. Amal, *Appl. Catal., B*, 2008, **78**, 1–10.
35 T. Sreethawong and S. Yoshikawa, *Catal. Commun.*, 2005, **6**, 661–668.
36 X. Chen and S. S. Mao, *Chem. Rev.*, 2007, **107**, 2891–2959.
37 J.-W. Yoon, T. Sasaki and N. Koshizaki, *Thin Solid Films*, 2005, **483**, 276–282.
38 B. Ohtani, K. Iwai, S.-I. Nishimoto and S. Sato, *J. Phys. Chem. B*, 1997, **101**, 3349–3359.
39 P. V. Kamat, *J. Phys. Chem. B*, 2002, **106**, 7729–7744.
40 V. Subramanian, E. E. Wolf and P. V. Kamat, *Langmuir*, 2002, **19**, 469–474.
41 G. L. Chiarello, E. Selli and L. Forni, *Appl. Catal., B*, 2008, **84**, 332–339.
42 G. L. Chiarello, M. H. Aguirre and E. Selli, *J. Catal.*, 2010, **273**, 182–190.
43 M. Sadeghi, W. Liu, T. G. Zhang, P. Stavropoulos and B. Levy, *J. Phys. Chem.*, 1996, **100**, 19466–19474.
44 M.-C. Wu, J. Hiltunen, A. Sápi, A. Avila, W. Larsson, H.-C. Liao, M. Huuhtanen, G. Tóth, A. Shchukarev, N. Laufer, Á. Kukovecz, Z. Kónya, J.-P. Mikkola, R. Keiski, W.-F. Su, Y.-F. Chen, H. Jantunen, P. M. Ajayan, R. Vajtai and K. Kordás, *ACS Nano*, 2011, **5**, 5025–5030.
45 V. Subramanian, E. Wolf and P. V. Kamat, *J. Phys. Chem. B*, 2001, **105**, 11439–11446.
46 T. Hirakawa and P. V. Kamat, *Langmuir*, 2004, **20**, 5645–5647.
47 J. Bisquert, A. Zaban and P. Salvador, *J. Phys. Chem. B*, 2002, **106**, 8774–8782.
48 A. Wood, M. Giersig and P. Mulvaney, *J. Phys. Chem. B*, 2001, **105**, 8810–8815.
49 V. Subramanian, E. E. Wolf and P. V. Kamat, *J. Phys. Chem. B*, 2003, **107**, 7479–7485.
50 G. Burgeth and H. Kisch, *Coord. Chem. Rev.*, 2002, **230**, 41–47.
51 E. Hussain, I. Majeed, M. A. Nadeem, A. Iqbal, Y. Chen, M. Choucair, R. Jin and M. A. Nadeem, *J. Environ. Chem. Eng.*, 2019, **7**, 102729.
52 V. Subramanian, E. E. Wolf and P. V. Kamat, *J. Am. Chem. Soc.*, 2004, **126**, 4943–4950.
53 S. Chen, R. S. Ingram, M. J. Hostetler, J. J. Pietron, R. W. Murray, T. Gregory Schaaff, J. T. Khoury, M. M. Alvarez and R. L. Whetten, *Science*, 1998, **280**, 2098–2101.
54 M. Jakob, H. Levanon and P. V. Kamat, *Nano Lett.*, 2003, **3**, 353–358.
55 H. Gerischer, *J. Phys. Chem.*, 1984, **88**, 6096–6097.
56 D. Y. C. Leung, X. Fu, C. Wang, M. Ni, M. K. H. Leung, X. Wang and X. Fu, *ChemSusChem*, 2010, **3**, 681–694.
57 J. Y. Park, J. Renzas, A. Contreras and G. A. Somorjai, *Top Catal.*, 2007, **46**, 217–222.
58 P. Gomathisankar, D. Yamamoto, H. Katsumata, T. Suzuki and S. Kaneco, *Int. J. Hydrogen Energy*, 2013, **38**, 5517–5524.
59 B. Kraeutler and A. J. Bard, *J. Am. Chem. Soc.*, 1978, **100**, 4317–4318.
60 M.-C. Wu, A. Sápi, A. Avila, M. Szabó, J. Hiltunen, M. Huuhtanen, G. Tóth, Á. Kukovecz, Z. Kónya, R. Keiski, W.-F. Su, H. Jantunen and K. Kordás, *Nano Res.*, 2011, **4**, 360–369.
61 G. Žerjav, M. Roškarič, J. Zavašnik, J. Kovač and A. Pintar, *Appl. Surf. Sci.*, 2022, **579**, 152196.
62 A. Wang, S. Wu, J. Dong, R. Wang, J. Wang, J. Zhang, S. Zhong and S. Bai, *Chem. Eng. J.*, 2021, **404**, 127145.
63 X. Ma, X. Wu, Y. Wang and Y. Dai, *Phys. Chem. Chem. Phys.*, 2017, **19**, 18750–18756.
64 M. A. Nadeem, M. Al-Oufi, A. K. Wahab, D. Anjum and H. Idriss, *ChemistrySelect*, 2017, **2**, 2754–2762.
65 M. A. El-Sayed, *Acc. Chem. Res.*, 2001, **34**, 257–264.
66 S. S. Rayalu, D. Jose, M. V. Joshi, P. A. Mangrulkar, K. Shrestha and K. Klabunde, *Appl. Catal., B*, 2013, **142**, 684–693.
67 W.-J. An, W.-N. Wang, B. Ramalingam, S. Mukherjee, B. Daubayev, S. Gangopadhyay and P. Biswas, *Langmuir*, 2012, **28**, 7528–7534.
68 U. Kreibig and L. Genzel, *Surf. Sci.*, 1985, **156**, 678–700.
69 I. Majeed, M. A. Nadeem, E. Hussain, A. Badshah, R. Gilani and M. A. Nadeem, *Int. J. Hydrogen Energy*, 2017, **42**, 3006–3018.
70 E. Thimsen, F. Le Formal, M. Grätzel and S. C. Warren, *Nano Lett.*, 2010, **11**, 35–43.
71 D. B. Ingram and S. Linic, *J. Am. Chem. Soc.*, 2011, **133**, 5202–5205.
72 M. Rycenga, C. M. Cobley, J. Zeng, W. Li, C. H. Moran, Q. Zhang, D. Qin and Y. Xia, *Chem. Rev.*, 2011, **111**, 3669–3712.
73 S. i Naya, A. Inoue and H. Tada, *ChemPhysChem*, 2011, **12**, 2719–2723.
74 S. Oros-Ruiz, R. Zanella, R. López, A. Hernández-Gordillo and R. Gómez, *J. Hazard. Mater.*, 2013, **263**(Part 1), 2–10.
75 M. A. Khan, M. Al-Oufi, A. Toseef, M. A. Nadeem and H. Idriss, *Catal. Lett.*, 2018, **148**, 1–10.
76 J. Jana, M. Ganguly and T. Pal, *RSC Adv.*, 2016, **6**, 86174–86211.
77 Y. Xia, Y. Xiong, B. Lim and S. E. Skrabalak, *Angew. Chem., Int. Ed.*, 2009, **48**, 60–103.
78 N. G. Khlebtsov, L. A. Trachuk and A. G. Melnikov, 2004.
79 A. Alekseeva, V. Bogatyrev, B. Khlebtsov, A. Mel'Nikov, L. Dykman and N. Khlebtsov, *Colloid J.*, 2006, **68**, 661–678.
80 N. Khlebtsov, L. Trachuk and A. Mel'nikov, *Opt. Spectrosc.*, 2005, **98**, 77–83.
81 Y. Tian and T. Tatsuma, *J. Am. Chem. Soc.*, 2005, **127**, 7632–7637.
82 C. U. Gomes Silva, R. Juárez, T. Marino, R. Molinari and H. García, *J. Am. Chem. Soc.*, 2010, **133**, 595–602.
83 X. Zhou, C. Hu, X. Hu, T. Peng and J. Qu, *J. Phys. Chem. C*, 2010, **114**, 2746–2750.
84 E. Kowalska, O. O. P. Mahaney, R. Abe and B. Ohtani, *Phys. Chem. Chem. Phys.*, 2010, **12**, 2344–2355.
85 M. K. Kumar, S. Krishnamoorthy, L. K. Tan, S. Y. Chiam, S. Tripathy and H. Gao, *ACS Catal.*, 2011, **1**, 300–308.
86 Y. Tian and T. Tatsuma, *Chem. Commun.*, 2004, 1810–1811.
87 A. Primo, T. Marino, A. Corma, R. Molinari and H. Garcia, *J. Am. Chem. Soc.*, 2011, **133**, 6930–6933.
88 S. Mukherjee, F. Libisch, N. Large, O. Neumann, L. V. Brown, J. Cheng, J. B. Lassiter, E. A. Carter, P. Nordlander and N. J. Halas, *Nano Lett.*, 2013, **13**, 240–247.

89 S. Mukherjee, L. Zhou, A. M. Goodman, N. Large, C. Ayala-Orozco, Y. Zhang, P. Nordlander and N. J. Halas, *J. Am. Chem. Soc.*, 2014, **136**, 64–67.
90 R. Sundararaman, P. Narang, A. S. Jermyn, W. A. Goddard III and H. A. Atwater, *Nat. Commun.*, 2014, **5**, 1–8.
91 A. M. Brown, R. Sundararaman, P. Narang, W. A. Goddard III and H. A. Atwater, *ACS Nano*, 2016, **10**, 957–966.
92 P. Narang, R. Sundararaman and H. A. Atwater, *Nanophotonics*, 2016, **5**, 96–111.
93 S. M. Kim, S. W. Lee, S. Y. Moon and J. Y. Park, *J. Phys.: Condens. Matter*, 2016, **28**, 254002.
94 J. Y. Park, S. M. Kim, H. Lee and I. I. Nedrygailov, *Acc. Chem. Res.*, 2015, **48**, 2475–2483.
95 J. S. DuChene, G. Tagliabue, A. J. Welch, W.-H. Cheng and H. A. Atwater, *Nano Lett.*, 2018, **18**, 2545–2550.
96 A. Primo, A. Corma and H. García, *Phys. Chem. Chem. Phys.*, 2011, **13**, 886–910.
97 R. Amrollahi, M. S. Hamdy and G. Mul, *J. Catal.*, 2014, **319**, 194–199.
98 Z. W. Seh, S. Liu, M. Low, S. Y. Zhang, Z. Liu, A. Mlayah and M. Y. Han, *Adv. Mater.*, 2012, **24**, 2310–2314.
99 S. Linic, P. Christopher and D. B. Ingram, *Nat. Mater.*, 2011, **10**, 911–921.
100 P. Christopher, D. B. Ingram and S. Linic, *J. Phys. Chem. C*, 2010, **114**, 9173–9177.
101 K. Awazu, M. Fujimaki, C. Rockstuhl, J. Tominaga, H. Murakami, Y. Ohki, N. Yoshida and T. Watanabe, *J. Am. Chem. Soc.*, 2008, **130**, 1676–1680.
102 Z. Liu, W. Hou, P. Pavaskar, M. Aykol and S. B. Cronin, *Nano Lett.*, 2011, **11**, 1111–1116.
103 P. Christopher, H. Xin and S. Linic, *Nat. Chem.*, 2011, **3**, 467–472.
104 D. B. Ingram, P. Christopher, J. L. Bauer and S. Linic, *ACS Catal.*, 2011, **1**, 1441–1447.
105 C. Burda, X. Chen, R. Narayanan and M. A. El-Sayed, *Chem. Rev.*, 2005, **105**, 1025–1102.
106 D. D. Evanoff and G. Chumanov, *ChemPhysChem*, 2005, **6**, 1221–1231.
107 M. A. Nadeem and H. Idriss, *Appl. Catal., B*, 2021, **284**, 119736.
108 M. Ghoussoub, M. Xia, P. N. Duchesne, D. Segal and G. Ozin, *Energy Environ. Sci.*, 2019, **12**, 1122–1142.
109 M. A. Nadeem and H. Idriss, *Chem. Commun.*, 2018, **54**, 5197–5200.
110 A. A. Upadhye, I. Ro, X. Zeng, H. J. Kim, I. Tejedor, M. A. Anderson, J. A. Dumesic and G. W. Huber, *Catal. Sci. Technol.*, 2015, **5**, 2590–2601.
111 T. H. Tan, J. Scott, Y. H. Ng, R. A. Taylor, K.-F. Aguey-Zinsou and R. Amal, *ACS Catal.*, 2016, **6**, 1870–1879.
112 J. C. Kennedy III and A. K. Datye, *J. Catal.*, 1998, **179**, 375–389.
113 R. Song, B. Luo and D. Jing, *Efficient photothermal catalytic hydrogen production over nonplasmonic Pt metal supported on TiO_2,* SPIE, 2016.
114 W. Chanmanee, M. F. Islam, B. H. Dennis and F. M. MacDonnell, *Proc. Natl. Acad. Sci. U. S. A.*, 2016, **113**, 2579–2584.
115 Y. H. Hu, *Angew. Chem., Int. Ed.*, 2012, **51**, 12410–12412.
116 Y. Huang, C. T. Rettner, D. J. Auerbach and A. M. Wodtke, *Science*, 2000, **290**, 111–114.
117 J. B. Joo, R. Dillon, I. Lee, Y. Yin, C. J. Bardeen and F. Zaera, *Proc. Natl. Acad. Sci. U. S. A.*, 2014, **111**, 7942–7947.
118 M. Bowker, P. R. Davies and L. S. Al-Mazroai, *Catal. Lett.*, 2008, **128**, 253.
119 M. Bowker, *Green Chem.*, 2011, **13**, 2235–2246.
120 J. Kennedy, W. Jones, D. J. Morgan, M. Bowker, L. Lu, C. J. Kiely, P. P. Wells and N. Dimitratos, *Catal., Struct. React.*, 2015, **1**, 35–43.
121 J. Greaves, L. Al-Mazroai, A. Nuhu, P. Davies and M. Bowker, *Gold Bull.*, 2006, **39**, 216–219.
122 F. Boccuzzi, A. Chiorino and M. Manzoli, *J. Power Sources*, 2003, **118**, 304–310.
123 S. Lee, J. Scott, K. Chiang and R. Amal, *J. Nanopart. Res.*, 2009, **11**, 209–219.
124 M. R. Hoffmann, S. T. Martin, W. Choi and D. W. Bahnemann, *Chem. Rev.*, 1995, **95**, 69–96.
125 T. Sakata and T. Kawai, *Chem. Phys. Lett.*, 1981, **80**, 341–344.
126 T. Maruyama and T. Nishimoto, *Ind. Eng. Chem. Res.*, 1991, **30**, 1634–1638.
127 A. L. Linsebigler, G. Lu and J. T. Yates, *Chem. Rev.*, 1995, **95**, 735–758.
128 G. R. Bamwenda, S. Tsubota, T. Nakamura and M. Haruta, *J. Photochem. Photobiol., A*, 1995, **89**, 177–189.
129 A. Naldoni, M. D'Arienzo, M. Altomare, M. Marelli, R. Scotti, F. Morazzoni, E. Selli and V. Dal Santo, *Appl. Catal., B*, 2013, **130–131**, 239–248.
130 T. Kawai and T. Sakata, 1980.
131 W. Sun, S. Zhang, Z. Liu, C. Wang and Z. Mao, *Int. J. Hydrogen Energy*, 2008, **33**, 1112–1117.
132 B. Ohtani, *Chem. Lett.*, 2008, **37**, 216–229.
133 N. Lakshminarasimhan, E. Bae and W. Choi, *J. Phys. Chem. C*, 2007, **111**, 15244–15250.
134 W. Fan, Q. Zhang and Y. Wang, *Phys. Chem. Chem. Phys.*, 2013, **15**, 2632–2649.
135 P. Wei, J. Liu and Z. Li, *Ceram. Int.*, 2013, **39**, 5387–5391.
136 J.-J. Zou, H. He, L. Cui and H.-Y. Du, *Int. J. Hydrogen Energy*, 2007, **32**, 1762–1770.
137 J. Xing, Y. H. Li, H. B. Jiang, Y. Wang and H. G. Yang, *Int. J. Hydrogen Energy*, 2014, **39**, 1237–1242.
138 J. Xing, H. B. Jiang, J. F. Chen, Y. H. Li, L. Wu, S. Yang, L. R. Zheng, H. F. Wang, P. Hu and H. J. Zhao, *J. Mater. Chem. A*, 2013, **1**, 15258–15264.
139 J. S. Jang, S. H. Choi, H. G. Kim and J. S. Lee, *J. Phys. Chem. C*, 2008, **112**, 17200–17205.
140 S. Tabata, H. Nishida, Y. Masaki and K. Tabata, *Catal. Lett.*, 1995, **34**, 245–249.
141 S. Sato and J. White, *Chem. Phys. Lett.*, 1980, **72**, 83–86.
142 M. Matsuoka, M. Kitano, M. Takeuchi, K. Tsujimaru, M. Anpo and J. M. Thomas, *Catal. Today*, 2007, **122**, 51–61.
143 K. Sayama and H. Arakawa, *J. Chem. Soc., Faraday Trans.*, 1997, **93**, 1647–1654.

144 S. C. Moon, H. Mametsuka, E. Suzuki and Y. Nakahara, *Catal. Today*, 1998, **45**, 79–84.
145 R. Abe, K. Sayama and H. Arakawa, *Chem. Phys. Lett.*, 2003, **371**, 360–364.
146 M. J. Hostetler, S. J. Green, J. J. Stokes and R. W. Murray, *J. Am. Chem. Soc.*, 1996, **118**, 4212–4213.
147 B. I. Ipe, K. G. Thomas, S. Barazzouk, S. Hotchandani and P. V. Kamat, *J. Phys. Chem. B*, 2001, **106**, 18–21.
148 T. Ung, M. Giersig, D. Dunstan and P. Mulvaney, *Langmuir*, 1997, **13**, 1773–1782.
149 P. V. Kamat, S. Barazzouk and S. Hotchandani, *Angew. Chem., Int. Ed.*, 2002, **41**, 2764–2767.
150 M. Haruta, *Catal. Today*, 1997, **36**, 153–166.
151 N. Chandrasekharan and P. V. Kamat, *J. Phys. Chem. B*, 2000, **104**, 10851–10857.
152 J. T. Carneiro, C.-C. Yang, J. A. Moma, J. A. Moulijn and G. Mul, *Catal. Lett.*, 2009, **129**, 12–19.
153 E. Kowalska, S. Rau and B. Ohtani, *J. Nanotechnol.*, 2012, **2012**, 361853.
154 S. S. Rayalu, D. Jose, M. V. Joshi, P. A. Mangrulkar, K. Shrestha and K. Klabunde, *Appl. Catal., B*, 2013, **142–143**, 684–693.
155 G. R. Bamwenda, S. Tsubota, T. Nakamura and M. Haruta, *J. Photochem. Photobiol., A*, 1995, **89**, 177–189.
156 C. J. Orendorff, T. K. Sau and C. J. Murphy, *Small*, 2006, **2**, 636–639.
157 M. M. Alvarez, J. T. Khoury, T. G. Schaaff, M. N. Shafigullin, I. Vezmar and R. L. Whetten, *J. Phys. Chem. B*, 1997, **101**, 3706–3712.
158 C. T. Yip, H. Huang, L. Zhou, K. Xie, Y. Wang, T. Feng, J. Li and W. Y. Tam, *Adv. Mater.*, 2011, **23**, 5624–5628.
159 Y. Xia, B. Gates and Z. Y. Li, *Adv. Mater.*, 2001, **13**, 409–413.
160 B. Hatton, L. Mishchenko, S. Davis, K. H. Sandhage and J. Aizenberg, *Proc. Natl. Acad. Sci. U. S. A.*, 2010, **107**, 10354–10359.
161 M. Qi, E. Lidorikis, P. T. Rakich, S. G. Johnson, J. Joannopoulos, E. P. Ippen and H. I. Smith, *Nature*, 2004, **429**, 538–542.
162 S. Noda, K. Tomoda, N. Yamamoto and A. Chutinan, *Science*, 2000, **289**, 604–606.
163 J. H. Lee, C. H. Kim, K. M. Ho and K. Constant, *Adv. Mater.*, 2005, **17**, 2481–2485.
164 S. R. Kennedy, M. J. Brett, O. Toader and S. John, *Nano Lett.*, 2002, **2**, 59–62.
165 A. S. Dimitrov and K. Nagayama, *Langmuir*, 1996, **12**, 1303–1311.
166 S. Y. Lim, C. S. Law, L. Liu, M. Markovic, C. Hedrich, R. H. Blick, A. D. Abell, R. Zierold and A. Santos, *Catalysts*, 2019, **9**, 988.
167 E. Yablonovitch, T. Gmitter and K.-M. Leung, *Phys. Rev. Lett.*, 1991, **67**, 2295.
168 J. Fleming and S.-Y. Lin, *Opt. Lett.*, 1999, **24**, 49–51.
169 Z. Zhang, L. Zhang, M. N. Hedhili, H. Zhang and P. Wang, *Nano Lett.*, 2012, **13**, 14–20.
170 G. Waterhouse, A. Wahab, M. Al-Oufi, V. Jovic, D. Anjum, D. Sun-Waterhouse, J. Llorca and H. Idriss, *Sci. Rep.*, 2013, **3**, 2849.
171 M.-C. Wu, J. Hiltunen, A. Sápi, A. Avila, W. Larsson, H.-C. Liao, M. Huuhtanen, G. Z. Tóth, A. Shchukarev and N. Laufer, *ACS Nano*, 2011, **5**, 5025–5030.
172 R. Su, R. Tiruvalam, Q. He, N. Dimitratos, L. Kesavan, C. Hammond, J. A. Lopez-Sanchez, R. Bechstein, C. J. Kiely and G. J. Hutchings, *ACS Nano*, 2012, **6**, 6284–6292.
173 M.-C. Wu, P.-H. Lee and D.-L. Lee, *Int. J. Hydrogen Energy*, 2015, **40**, 4558–4566.
174 A. A. Ismail, S. A. Al-Sayari and D. Bahnemann, *Catal. Today*, 2013, **209**, 2–7.
175 Z. H. Al-Azri, W.-T. Chen, A. Chan, V. Jovic, T. Ina, H. Idriss and G. I. Waterhouse, *J. Catal.*, 2015, **329**, 355–367.
176 S. Nishimura, *Handbook of heterogeneous catalytic hydrogenation for organic synthesis*, Wiley, New York, 2001.
177 R. Su, R. Tiruvalam, A. J. Logsdail, Q. He, C. A. Downing, M. T. Jensen, N. Dimitratos, L. Kesavan, P. P. Wells and R. Bechstein, *ACS Nano*, 2014, **8**, 3490–3497.
178 A. Gluhoi, X. Tang, P. Marginean and B. Nieuwenhuys, *Top Catal.*, 2006, **39**, 101–110.
179 L.-H. Chang, Y.-W. Chen and N. Sasirekha, *Ind. Eng. Chem. Res.*, 2008, **47**, 4098–4105.
180 Z.-P. Liu, S. J. Jenkins and D. A. King, *Phys. Rev. Lett.*, 2004, **93**, 156102.
181 A. C. Gluhoi and B. E. Nieuwenhuys, *Catal. Today*, 2007, **122**, 226–232.
182 E. Hussain, I. Majeed, M. A. Nadeem, A. Badshah, Y. Chen, M. A. Nadeem and R. Jin, *J. Phys. Chem. C*, 2016, **120**, 17205–17213.
183 K. Yang, Y. Zhang, Y. Li, P. Huang, X. Chen, W. Dai and X. Fu, *Appl. Catal., B*, 2016, **183**, 206–215.
184 S. Zhang, H. Wang, M. Yeung, Y. Fang, H. Yu and F. Peng, *Int. J. Hydrogen Energy*, 2013, **38**, 7241–7245.
185 J. Yu and J. Ran, *Energy Environ. Sci.*, 2011, **4**, 1364–1371.
186 S. Xu and D. D. Sun, *Int. J. Hydrogen Energy*, 2009, **34**, 6096–6104.
187 D. P. Singh, N. R. Neti, A. S. K. Sinha and O. N. Srivastava, *J. Phys. Chem. C*, 2007, **111**, 1638–1645.
188 S. Xu, J. Ng, X. Zhang, H. Bai and D. D. Sun, *Int. J. Hydrogen Energy*, 2010, **35**, 5254–5261.
189 J. Kondo, *Chem. Commun.*, 1998, 357–358.
190 J. Morales, J. Espinos, A. Caballero, A. Gonzalez-Elipe and J. A. Mejias, *J. Phys. Chem. B*, 2005, **109**, 7758–7765.
191 Y. Sui, W. Fu, H. Yang, Y. Zeng, Y. Zhang, Q. Zhao, Y. Li, X. Zhou, Y. Leng and M. Li, *Cryst. Growth Des.*, 2009, **10**, 99–108.
192 J.-N. Nian, C.-C. Hu and H. Teng, *Int. J. Hydrogen Energy*, 2008, **33**, 2897–2903.
193 H. Bahruji, M. Bowker, C. Brookes, P. R. Davies and I. Wawata, *Appl. Catal., A*, 2013, **454**, 66–73.
194 B. Meyer, A. Polity, D. Reppin, M. Becker, P. Hering, P. Klar, T. Sander, C. Reindl, J. Benz and M. Eickhoff, *Phys. Status Solidi B*, 2012, **249**, 1487–1509.
195 H. Gerischer, *J. Electroanal. Chem. Interfacial Electrochem.*, 1977, **82**, 133–143.
196 A. Paracchino, J. C. Brauer, J.-E. Moser, E. Thimsen and M. Graetzel, *J. Phys. Chem. C*, 2012, **116**, 7341–7350.

197 A. Paracchino, V. Laporte, K. Sivula, M. Grätzel and E. Thimsen, *Nat. Mater.*, 2011, **10**, 456–461.
198 W.-W. So, K.-J. Kim and S.-J. Moon, *Int. J. Hydrogen Energy*, 2004, **29**, 229–234.
199 J. S. Jang, S. M. Ji, S. W. Bae, H. C. Son and J. S. Lee, *J. Photochem. Photobiol., A*, 2007, **188**, 112–119.
200 J. S. Jang, H. G. Kim, U. A. Joshi, J. W. Jang and J. S. Lee, *Int. J. Hydrogen Energy*, 2008, **33**, 5975–5980.
201 J. Cao, B. Xu, H. Lin, B. Luo and S. Chen, *Dalton Trans.*, 2012, **41**, 11482–11490.
202 J. Jiang, X. Zhang, P. Sun and L. Zhang, *J. Phys. Chem. C*, 2011, **115**, 20555–20564.
203 D. Sarkar, C. K. Ghosh, S. Mukherjee and K. K. Chattopadhyay, *ACS Appl. Mater. Interfaces*, 2012, **5**, 331–337.
204 X. Wang, G. Liu, G. Q. Lu and H.-M. Cheng, *Int. J. Hydrogen Energy*, 2010, **35**, 8199–8205.
205 C. Shifu, Z. Sujuan, L. Wei and Z. Wei, *J. Nanosci. Nanotechnol.*, 2009, **9**, 4397–4403.
206 Y. Chen, J. C. Crittenden, S. Hackney, L. Sutter and D. W. Hand, *Environ. Sci. Technol.*, 2005, **39**, 1201–1208.
207 L. Zheng, Y. Zheng, C. Chen, Y. Zhan, X. Lin, Q. Zheng, K. Wei and J. Zhu, *Inorg. Chem.*, 2009, **48**, 1819–1825.
208 L. Sinatra, A. LaGrow, W. Peng, A. Kirmani, A. Amassian, H. Idriss and O. Bakr, *J. Catal.*, 2015, **322**, 109–117.
209 W.-Y. Cheng, T.-H. Yu, K.-J. Chao and S.-Y. Lu, *Int. J. Hydrogen Energy*, 2013, **38**, 9665–9672.
210 L. Sinatra, A. P. LaGrow, W. Peng, A. R. Kirmani, A. Amassian, H. Idriss and O. M. Bakr, *J. Catal.*, 2015, **322**, 109–117.
211 S. Zhang, B. Peng, S. Yang, Y. Fang and F. Peng, *Int. J. Hydrogen Energy*, 2013, **38**, 13866–13871.
212 Z. Xi, C. Li, L. Zhang, M. Xing and J. Zhang, *Int. J. Hydrogen Energy*, 2014, **39**, 6345–6353.
213 K. Lalitha, G. Sadanandam, V. D. Kumari, M. Subrahmanyam, B. Sreedhar and N. Y. Hebalkar, *J. Phys. Chem. C*, 2010, **114**, 22181–22189.
214 I. Majeed, M. A. Nadeem, A. Badshah, F. K. Kanodarwala, H. Ali, M. A. Khan, J. A. Stride and M. A. Nadeem, *Catal. Sci. Technol.*, 2017, **7**, 677–686.
215 J. Bandara, C. P. K. Udawatta and C. S. K. Rajapakse, *Photochem. Photobiol. Sci.*, 2005, **4**, 857–861.
216 H.-J. Choi and M. Kang, *Int. J. Hydrogen Energy*, 2007, **32**, 3841–3848.
217 J. Bandara, C. Udawatta and C. Rajapakse, *Photochem. Photobiol. Sci.*, 2005, **4**, 857–861.
218 S. Xu and D. D. Sun, *Int. J. Hydrogen Energy*, 2009, **34**, 6096–6104.
219 L. Yoong, F. K. Chong and B. K. Dutta, *Energy*, 2009, **34**, 1652–1661.
220 M. A. S. Khan, M. K. Kesharwani, T. Bandyopadhyay and B. Ganguly, *J. Mol. Graphics Modell.*, 2009, **28**, 177–182.
221 S. Xu, A. J. Du, J. Liu, J. Ng and D. D. Sun, *Int. J. Hydrogen Energy*, 2011, **36**, 6560–6568.
222 J. Yu, Y. Hai and M. Jaroniec, *J. Colloid Interface Sci.*, 2011, **357**, 223–228.
223 W.-T. Chen, V. Jovic, D. Sun-Waterhouse, H. Idriss and G. I. N. Waterhouse, *Int. J. Hydrogen Energy*, 2013, **38**, 15036–15048.
224 M. Jung, J. Scott, Y. H. Ng, Y. Jiang and R. Amal, *Int. J. Hydrogen Energy*, 2014, **39**, 12499–12506.
225 I. Majeed, M. A. Nadeem, A. Badshah, F. K. Kanodarwala, H. Ali, M. A. Khan, J. A. Stride and M. A. Nadeem, *Catal. Sci. Technol.*, 2017, **7**, 677–686.
226 J. Yu and J. Ran, *Energy Environ. Sci.*, 2011, **4**, 1364–1371.
227 V. Gombac, L. Sordelli, T. Montini, J. J. Delgado, A. Adamski, G. Adami, M. Cargnello, S. Bernal and P. Fornasiero, *J. Phys. Chem. A*, 2010, **114**, 3916–3925.
228 T. Montini, V. Gombac, L. Sordelli, J. J. Delgado, X. Chen, G. Adami and P. Fornasiero, *ChemCatChem*, 2011, **3**, 574–577.
229 C. Ampelli, R. Passalacqua, C. Genovese, S. Perathoner, G. Centi, T. Montini, V. Gombac, J. J. Delgado Jaen and P. Fornasiero, *RSC Adv.*, 2013, **3**, 21776–21788.
230 J. Yu, Y. Hai and B. Cheng, *J. Phys. Chem. C*, 2011, **115**, 4953–4958.
231 W.-T. Chen, A. Chan, D. Sun-Waterhouse, T. Moriga, H. Idriss and G. I. Waterhouse, *J. Catal.*, 2015, **326**, 43–53.
232 A. Domingo, A. Rodríguez-Fortea, M. Swart, C. de Graaf and R. Broer, *Phys. Rev. B: Condens. Matter Mater. Phys.*, 2012, **85**, 155143.
233 A. L. Linsebigler, G. Lu and J. T. Yates Jr, *Chem. Rev.*, 1995, **95**, 735–758.
234 J. A. Rodriguez, J. C. Hanson, A. I. Frenkel, J. Y. Kim and M. Pérez, *J. Am. Chem. Soc.*, 2002, **124**, 346–354.
235 S.-I. Fujita, H. Kawamori, D. Honda, H. Yoshida and M. Arai, *Appl. Catal., B*, 2016, **181**, 818–824.
236 W.-T. Chen, A. Chan, D. Sun-Waterhouse, T. Moriga, H. Idriss and G. I. N. Waterhouse, *J. Catal.*, 2015, **326**, 43–53.
237 W. Fritzsche and T. A. Taton, *Nanotechnology*, 2003, **14**, R63.
238 M. Hu, J. Chen, Z.-Y. Li, L. Au, G. V. Hartland, X. Li, M. Marquez and Y. Xia, *Chem. Soc. Rev.*, 2006, **35**, 1084–1094.
239 S. Pillai, K. Catchpole, T. Trupke and M. Green, *J. Appl. Phys.*, 2007, **101**, 093105.
240 R. Narayanan and M. A. El-Sayed, *J. Phys. Chem. B*, 2005, **109**, 12663–12676.
241 W. L. Barnes, A. Dereux and T. W. Ebbesen, *Nature*, 2003, **424**, 824–830.
242 M. Garcia, *J. Phys. D: Appl. Phys.*, 2012, **45**, 389501.
243 R. Kavitha and S. G. Kumar, *Chemurg. Pap.*, 2020, **74**, 717–756.
244 R. Wei, N. Tang, L. Jiang, J. Yang, J. Guo, X. Yuan, J. Liang, Y. Zhu, Z. Wu and H. Li, *Coord. Chem. Rev.*, 2022, **462**, 214500.
245 Y.-H. Li, J.-Y. Li and Y.-J. Xu, *Energy Chem.*, 2021, **3**, 100047.
246 R. Kavitha, P. M. Nithya and S. Girish Kumar, *Appl. Surf. Sci.*, 2020, **508**, 145142.
247 R. Kavitha and S. G. Kumar, *Mater. Sci. Semicond. Process.*, 2019, **93**, 59–91.
248 L. Li, Z. Xu, F. Liu, Y. Shao, J. Wang, H. Wan and S. Zheng, *J. Photochem. Photobiol., A*, 2010, **212**, 113–121.

249 M. Yamauchi, R. Abe, T. Tsukuda, K. Kato and M. Takata, *J. Am. Chem. Soc.*, 2011, **133**, 1150–1152.
250 Y. Mizukoshi, K. Sato, T. J. Konno and N. Masahashi, *Appl. Catal., B*, 2010, **94**, 248–253.
251 A. Gallo, M. Marelli, R. Psaro, V. Gombac, T. Montini, P. Fornasiero, R. Pievo and V. Dal Santo, *Green Chem.*, 2012, **14**, 330–333.
252 V. Dal Santo, A. Gallo, A. Naldoni, M. Guidotti and R. Psaro, *Catal. Today*, 2012, **197**, 190–205.
253 P. Montes-Navajas, M. Serra and H. Garcia, *Catal. Sci. Technol.*, 2013, **3**, 2252–2258.
254 N. Toshima and K. Hirakawa, *Appl. Surf. Sci.*, 1997, **121**, 534–537.
255 D. Wang and Y. Li, *Adv. Mater.*, 2011, **23**, 1044–1060.
256 L. Guczi, G. Boskovic and E. Kiss, *Catal. Rev.: Sci. Eng.*, 2010, **52**, 133–203.
257 H. Tada, F. Suzuki, S. Ito, T. Akita, K. Tanaka, T. Kawahara and H. Kobayashi, *J. Phys. Chem. B*, 2002, **106**, 8714–8720.
258 Z. Zhang, S.-W. Cao, Y. Liao and C. Xue, *Appl. Catal., B*, 2015, **162**, 204–209.
259 A. Wahab, S. Bashir, Y. Al-Salik and H. Idriss, *Appl. Petrochem. Res.*, 2014, **4**, 55–62.
260 P. Mulvaney, M. Giersig and A. Henglein, *J. Phys. Chem.*, 1992, **96**, 10419–10424.
261 D. O. Scanlon, C. W. Dunnill, J. Buckeridge, S. A. Shevlin, A. J. Logsdail, S. M. Woodley, C. R. A. Catlow, M. J. Powell, R. G. Palgrave and I. P. Parkin, *Nat. Mater.*, 2013, **12**, 798–801.
262 P. Zhou, Z. Li and Z. Zou, *Curr. Inorg. Chem.*, 2012, **2**, 184–193.
263 Z. Li, J. Liu, D. Wang, Y. Gao and J. Shen, *Int. J. Hydrogen Energy*, 2012, **37**, 6431–6437.
264 H. Husin, W.-N. Su, H.-M. Chen, C.-J. Pan, S.-H. Chang, J. Rick, W.-T. Chuang, H.-S. Sheu and B.-J. Hwang, *Green Chem.*, 2011, **13**, 1745–1754.
265 A. K. Agegnehu, C.-J. Pan, J. Rick, J.-F. Lee, W.-N. Su and B.-J. Hwang, *J. Mater. Chem.*, 2012, **22**, 13849–13854.
266 H. Tian, S.-Z. Kang, X. Li, L. Qin, M. Ji and J. Mu, *Sol. Energy Mater. Sol. Cells*, 2015, **134**, 309–317.
267 I. Majeed, M. A. Nadeem, E. Hussain, G. I. Waterhouse, A. Badshah, A. Iqbal, M. A. Nadeem and H. Idriss, *ChemCatChem*, 2016, **8**, 3146–3155.
268 H. Nishiyama and Y. Inoue, *J. Phys. Chem. B*, 2003, **107**, 8738–8741.
269 R. J. Tayade, R. G. Kulkarni and R. V. Jasra, *Ind. Eng. Chem. Res.*, 2006, **45**, 5231–5238.
270 X.-J. Zheng, L.-F. Wei, Z.-H. Zhang, Q.-J. Jiang, Y.-J. Wei, B. Xie and M.-B. Wei, *Int. J. Hydrogen Energy*, 2009, **34**, 9033–9041.
271 M. Bowker, D. James, P. Stone, R. Bennett, N. Perkins, L. Millard, J. Greaves and A. Dickinson, *J. Catal.*, 2003, **217**, 427–433.
272 M. I. Litter, *Appl. Catal., B*, 1999, **23**, 89–114.
273 O. Carp, C. L. Huisman and A. Reller, *Prog. Solid State Chem.*, 2004, **32**, 33–177.
274 J. S. Jang, S. M. Ji, S. W. Bae, H. C. Son and J. S. Lee, *J. Photochem. Photobiol., A*, 2007, **188**, 112–119.
275 K. Sayama, R. Abe, H. Arakawa and H. Sugihara, *Catal. Commun.*, 2006, **7**, 96–99.
276 J.-J. Zou, C.-J. Liu, K.-L. Yu, D.-G. Cheng, Y.-P. Zhang, F. He, H.-Y. Du and L. Cui, *Chem. Phys. Lett.*, 2004, **400**, 520–523.
277 J.-J. Zou, H. He, L. Cui and H.-Y. Du, *Int. J. Hydrogen Energy*, 2007, **32**, 1762–1770.
278 Y. Mizukoshi, Y. Makise, T. Shuto, J. Hu, A. Tominaga, S. Shironita and S. Tanabe, *Ultrason. Sonochem.*, 2007, **14**, 387–392.
279 M. Murdoch, G. I. N. Waterhouse, M. A. Nadeem, J. B. Metson, M. A. Keane, R. F. Howe, J. Llorca and H. Idriss, *Nat. Chem.*, 2011, **3**, 489–492.
280 B.-W. Zhang, Y.-X. Wang, S.-L. Chou, H.-K. Liu and S.-X. Dou, *Small Methods*, 2019, **3**, 1800497.
281 S. Wei, A. Li, J.-C. Liu, Z. Li, W. Chen, Y. Gong, Q. Zhang, W.-C. Cheong, Y. Wang, L. Zheng, H. Xiao, C. Chen, D. Wang, Q. Peng, L. Gu, X. Han, J. Li and Y. Li, *Nat. Nanotechnol.*, 2018, **13**, 856–861.
282 Z. Zeng, Y. Su, X. Quan, W. Choi, G. Zhang, N. Liu, B. Kim, S. Chen, H. Yu and S. Zhang, *Nano Energy*, 2020, **69**, 104409.
283 P. Yin, T. Yao, Y. Wu, L. Zheng, Y. Lin, W. Liu, H. Ju, J. Zhu, X. Hong, Z. Deng, G. Zhou, S. Wei and Y. Li, *Angew. Chem., Int. Ed.*, 2016, **55**, 10800–10805.
284 L. Jiao and H.-L. Jiang, *Chem*, 2019, **5**, 786–804.
285 Y. Li, B. Li, D. Zhang, L. Cheng and Q. Xiang, *ACS Nano*, 2020, **14**, 10552–10561.
286 X. Li, W. Bi, L. Zhang, S. Tao, W. Chu, Q. Zhang, Y. Luo, C. Wu and Y. Xie, *Adv. Mater.*, 2016, **28**, 2427–2431.
287 J. Wang, Z. Li, Y. Wu and Y. Li, *Adv. Mater.*, 2018, **30**, 1801649.
288 Y. Yang, F. Li, J. Chen, J. Fan and Q. Xiang, *ChemSusChem*, 2020, **13**, 1979–1985.
289 H. Zhang, X. F. Lu, Z.-P. Wu and X. W. D. Lou, *ACS Cent. Sci.*, 2020, **6**, 1288–1301.
290 H. Huang, K. Shen, F. Chen and Y. Li, *ACS Catal.*, 2020, **10**, 6579–6586.
291 C. Gao, J. Low, R. Long, T. Kong, J. Zhu and Y. Xiong, *Chem. Rev.*, 2020, **120**, 12175–12216.
292 J. Li, Q. Guan, H. Wu, W. Liu, Y. Lin, Z. Sun, X. Ye, X. Zheng, H. Pan, J. Zhu, S. Chen, W. Zhang, S. Wei and J. Lu, *J. Am. Chem. Soc.*, 2019, **141**, 14515–14519.
293 X. Wang, H. He, Y. Chen, J. Zhao and X. Zhang, *Appl. Surf. Sci.*, 2012, **258**, 5863–5868.
294 H. G. Yang, C. H. Sun, S. Z. Qiao, J. Zou, G. Liu, S. C. Smith, H. M. Cheng and G. Q. Lu, *Nature*, 2008, **453**, 638–641.
295 S. Selçuk and A. Selloni, *J. Phys. Chem. C*, 2013, **117**, 6358–6362.
296 Y. Dai, C. M. Cobley, J. Zeng, Y. Sun and Y. Xia, *Nano Lett.*, 2009, **9**, 2455–2459.
297 W.-S. Wang, D.-H. Wang, W.-G. Qu, L.-Q. Lu and A.-W. Xu, *J. Phys. Chem. C*, 2012, **116**, 19893–19901.
298 S. G. Kumar and L. G. Devi, *J. Phys. Chem. A*, 2011, **115**, 13211–13241.
299 A. Selloni, *Nat. Mater.*, 2008, **7**, 613–615.
300 X.-Q. Gong and A. Selloni, *J. Phys. Chem. B*, 2005, **109**, 19560–19562.

301 A. Vittadini, A. Selloni, F. Rotzinger and M. Grätzel, *Phys. Rev. Lett.*, 1998, **81**, 2954.
302 P. Zawadzki, A. B. Laursen, K. W. Jacobsen, S. Dahl and J. Rossmeisl, *Energy Environ. Sci.*, 2012, **5**, 9866–9869.
303 B. Enright and D. Fitzmaurice, *J. Phys. Chem.*, 1996, **100**, 1027–1035.
304 J. Yu, L. Qi and M. Jaroniec, *J. Phys. Chem. C*, 2010, **114**, 13118–13125.
305 W.-K. Wang, J.-J. Chen, Z.-Z. Lou, S. Kim, M. Fujitsuka, H.-Q. Yu and T. Majima, *Proc. Natl. Acad. Sci. U. S. A.*, 2019, **116**, 18827–18833.
306 M. I. Litter, E. San Román, T. L. M. A. Grela, J. M. Meichtry and H. B. Rodríguez, *Visible Light-Active Photocatalysis*, 2018, 253–282, DOI: **10.1002/9783527808175.ch10**.
307 N. Manfredi, M. Monai, T. Montini, F. Peri, F. De Angelis, P. Fornasiero and A. Abbotto, *ACS Energy Lett.*, 2018, **3**, 85–91.
308 A. Dessì, M. Monai, M. Bessi, T. Montini, M. Calamante, A. Mordini, G. Reginato, C. Trono, P. Fornasiero and L. Zani, *ChemSusChem*, 2018, **11**, 793–805.
309 B. Cecconi, N. Manfredi, R. Ruffo, T. Montini, I. Romero-Ocaña, P. Fornasiero and A. Abbotto, *ChemSusChem*, 2015, **8**, 4216–4228.
310 A. Abbotto, N. Manfredi, C. Marinzi, F. De Angelis, E. Mosconi, J.-H. Yum, Z. Xianxi, M. K. Nazeeruddin and M. Grätzel, *Energy Environ. Sci.*, 2009, **2**, 1094–1101.
311 Z. Bian, T. Tachikawa, W. Kim, W. Choi and T. Majima, *J. Phys. Chem. C*, 2012, **116**, 25444–25453.
312 Z. Bian, T. Tachikawa, P. Zhang, M. Fujitsuka and T. Majima, *J. Am. Chem. Soc.*, 2014, **136**, 458–465.
313 X. Shi, Z. Lou, P. Zhang, M. Fujitsuka and T. Majima, *ACS Appl. Mater. Interfaces*, 2016, **8**, 31738–31745.
314 M. Zhu, X. Cai, M. Fujitsuka, J. Zhang and T. Majima, *Angew. Chem., Int. Ed.*, 2017, **56**, 2064–2068.
315 A. Nadeem, G. I. Waterhouse, J. Metson and H. Idriss, *Journal*, 2010, 7770.
316 H. Kisch and D. Bahnemann, *J. Phys. Chem. Lett.*, 2015, **6**, 1907–1910.
317 L. Y. Kunz, B. T. Diroll, C. J. Wrasman, A. R. Riscoe, A. Majumdar and M. Cargnello, *Energy Environ. Sci.*, 2019, **12**, 1657–1667.
318 J. Hoy, P. J. Morrison, L. K. Steinberg, W. E. Buhro and R. A. Loomis, *J. Phys. Chem. Lett.*, 2013, **4**, 2053–2060.
319 M. Melchionna and P. Fornasiero, *ACS Catal.*, 2020, **10**, 5493–5501.
320 J. Puskelova, L. Baia, A. Vulpoi, M. Baia, M. Antoniadou, V. Dracopoulos, E. Stathatos, K. Gabor, Z. Pap and V. Danciu, *Chem. Eng. J.*, 2014, **242**, 96–101.
321 S. Li, Y. Guo, L. Zhang, J. Wang, Y. Li, Y. Li and B. Wang, *J. Power Sources*, 2014, **252**, 21–27.
322 W. Qin, D. Zhang, D. Zhao, L. Wang and K. Zheng, *Chem. Commun.*, 2010, **46**, 2304–2306.
323 G. Feng, S. Liu, Z. Xiu, Y. Zhang, J. Yu, Y. Chen, P. Wang and X. Yu, *J. Phys. Chem. C*, 2008, **112**, 13692–13699.
324 J. Yu and J. Ran, *Energy Environ. Sci.*, 2011, **4**, 1364–1371.
325 X. Chen, L. Liu, P. Y. Yu and S. S. Mao, *Science*, 2011, **331**, 746–750.
326 S. S. Sahoo, S. Mansingh, P. Babu and K. Parida, *Nanoscale Adv.*, 2021, **3**, 5487–5524.
327 A. C. Fisher, L. M. Peter, E. A. Ponomarev, A. B. Walker and K. G. U. Wijayantha, *J. Phys. Chem. B*, 2000, **104**, 949–958.
328 O. K. Varghese, M. Paulose and C. A. Grimes, *Nat. Nanotechnol.*, 2009, **4**, 592–597.
329 M. Cargnello, T. Montini, S. Y. Smolin, J. B. Priebe, J. J. D. Jaén, V. V. T. Doan-Nguyen, I. S. McKay, J. A. Schwalbe, M.-M. Pohl, T. R. Gordon, Y. Lu, J. B. Baxter, A. Brückner, P. Fornasiero and C. B. Murray, *Proc. Natl. Acad. Sci. U. S. A.*, 2016, **113**, 3966–3971.
330 C. Wang, Q. Hu, J. Huang, C. Zhu, Z. Deng, H. Shi, L. Wu, Z. Liu and Y. Cao, *Appl. Surf. Sci.*, 2014, **292**, 161–164.
331 I. Cesar, A. Kay, J. A. Gonzalez Martinez and M. Grätzel, *J. Am. Chem. Soc.*, 2006, **128**, 4582–4583.
332 A. Selloni, *Nat. Mater.*, 2008, **7**, 613–615.
333 X.-Q. Gong and A. Selloni, *J. Phys. Chem. B*, 2005, **109**, 19560–19562.
334 A. Vittadini, A. Selloni, F. P. Rotzinger and M. Grätzel, *Phys. Rev. Lett.*, 1998, **81**, 2954–2957.
335 M. Alrushaid, M. A. Nadeem, K. A. Wahab and H. Idriss, *Catalysts*, 2021, **11**, 1030.